



11 ABSTRACT: Urban climate model evaluation often remains limited by a lack of trusted urban  
12 weather observations. The increasing density of personal weather stations (PWS) make them  
13 a potential rich source of data for urban climate studies that address the lack of representative  
14 urban weather observations. In our study, we demonstrate that PWS data not only improve urban  
15 climate models' evaluation, but can also serve for bias-correcting their output prior to any urban  
16 climate impact studies. After simulating near-surface air temperatures over London and south-  
17 east England during the hot summer of 2018 with the Weather Research Forecast (WRF) model  
18 and its Building Effect Parameterization with the Building Energy Model (BEP-BEM) activated,  
19 we evaluated the modelled temperatures against 407 urban PWS and showcased a heterogeneous  
20 spatial distribution of the model's cool bias that was not captured using official weather stations  
21 only. This finding indicated a need for spatially-explicit urban bias corrections of air temperatures,  
22 which we performed using an innovative method using machine learning to predict the models'  
23 biases in each urban grid cell. Our technique is the first to consider that urban temperatures are  
24 heterogeneously accurate in space and that this accuracy is not linearly correlated to the urban  
25 fraction. Our results showed that the bias-correction was beneficial to bias-correct daily-minimum,  
26 -mean, and -maximum temperatures in the cities. We recommend that urban climate modellers  
27 further investigate the use of PWS for model evaluation and derive a framework for bias-correction  
28 of urban climate simulations that can serve urban climate impact studies.

29 SIGNIFICANCE STATEMENT: Urban climate simulations are subject to spatially heteroge-  
30 neous biases in urban air temperatures. Common validation methods using official weather stations  
31 do not suffice for detecting these biases. Using a dense set of personal weather stations in London  
32 we detect these biases before proposing an innovative way for correcting them with machine learn-  
33 ing techniques. We argue that any urban climate impact study should use such technique if possible  
34 and that urban climate scientists should continue investigating paths to improve our methods.

## 35 **1. Introduction**

36 Although decades following the 1960s have seen an increase in the body of literature on urban  
37 climates (Oke et al. 2017), the scales of applicability and the transferability of their outcomes are  
38 often limited. This can partially be attributed to the lack of observations representative of the variety  
39 of existing urban climates in cities. To address this impediment, two major solutions were proposed  
40 over the past 20 years: firstly, the development of urban surface energy balance and climate models  
41 (e.g., Masson (2000), Martilli et al. (2002), Wouters et al. (2016)) that are coupled to regional  
42 climate models, and secondly, the increased interest towards crowd-sourced and low-cost weather  
43 sensors (e.g., Muller et al. (2015), Chapman et al. (2017), Fenner et al. (2017), Meier et al. (2017)).  
44 Indeed, after proper validation and parameterization, urbanized regional climate models, with  
45 their urban climate models (UCMs) activated, offer an unprecedented opportunity to represent the  
46 impact of cities on a wide variety of weather variables at very high spatial and temporal resolutions  
47 – an opportunity further supported by the recent development of global standardized land use  
48 land cover datasets designed for urban climate studies that permit their parameterization in cities  
49 formerly deprived of these data (see the World Urban Dataset and Access Portal Tool (WUDAPT)  
50 project; Ching et al. (2018), Demuzere et al. (2022)). Likewise, after proper filtering and quality  
51 control (Napoly et al. 2018; Fenner et al. 2021), crowd-sourced personal weather sensors (PWS)  
52 permit the extension of sensing networks into urban environments that were formerly not studied  
53 despite the fact that PWS often do not meet the standards imposed by official meteorological offices  
54 for implementation of weather stations.

55 Nonetheless, both these tools have limitations. For instance, PWS observations are of lower  
56 reliability and accuracy than official weather stations and cover only recent years, booming after  
57 2015 (Brousse et al. 2022). Relating the observed weather to the underlying environmental

58 characteristics can also be difficult, as requirements for the site description are modest to non-  
59 existent. Recent efforts have however managed to bridge this information gap by using earth  
60 observations, and in particular the universal standardized Local Climate Zones land-use land-cover  
61 classification (Stewart and Oke 2012) which permitted not only the study of key weather variables  
62 in cities, like near-surface air temperature (e.g., Fenner et al. (2019), Potgieter et al. (2021),  
63 Benjamin et al. (2021), Varentsov et al. (2021)), but also their prediction via machine learning  
64 (Venter et al. 2020, 2021). Though these mapping efforts, aided by the development of machine  
65 learning algorithms, are substantial achievements, better predictions were usually achieved at low  
66 temporal resolution (e.g., weekly or seasonally), thus calling for more research to be done in order  
67 to reach improved performance at daily or hourly time-steps. This research could help comparing  
68 the outputs of physical models, like UCMs, to predicted maps of urban-specific weather variables  
69 obtained via PWS.

70 Indeed, UCMs are computationally expensive, require complex and energy-consuming com-  
71 putational infrastructures, and require prior expert-knowledge to be properly used. For example,  
72 depending on the study in terms of city-location, domain dimension, horizontal and temporal scales,  
73 or meteorological variables of interest, users need to ascertain that their models are meaningfully  
74 parameterized with the right physical and dynamical schemes, and forced by representative initial  
75 and boundary atmospheric conditions. These requirements are usually verified through sensitivity  
76 tests performed before running real-case scenarios, where model outputs are compared against  
77 weather measurements obtained from official weather stations. Then, users balance the need for  
78 accuracy with computational limitations. Notwithstanding, hazardous uncertainties exist even af-  
79 ter sensitivity studies are performed, as shown by Bassett et al. (2020) who demonstrated that the  
80 starting time of the simulation had a noticeable impact on the modelled air temperature at 2 m in  
81 London during the summer 2018. Moreover, because of the lack of official weather stations in  
82 cities, measuring existing uncertainties per urban climate archetype is not feasible. This means that  
83 certain urban environments are poorly evaluated and hence modelled, assuming that UCMs will  
84 perform similarly under all constraints imposed by the variety of urban environments that compose  
85 a city. In face of this challenge, quality-checked crowd-sourced PWS allow monitoring for a range  
86 of urban environments. They can therefore serve the evaluation of UCMs, as Hammerberg et al.  
87 (2018) demonstrated over Vienna. But the potential of PWS may even be greater, particularly when

88 used jointly with or in parallel to UCMs. In fact, a recent study by Sgoff et al. (2022) improved  
89 the weather forecasting of the Icosahedral Nonhydrostatic Model (ICON; Zängl et al. (2015)) at  
90 a horizontal resolution of 2 km over Germany by assimilating the data provided by PWS for air  
91 temperature and relative humidity at 2 m height. Although data assimilation is done while UCMs  
92 are running, PWS could also be used to subsequently bias-correct urban climate simulations. To  
93 date, no study has explored how PWS could be used to bias-correct simulated urban climates  
94 despite the need for realistic urban weather data of present and future urban climates to perform  
95 impact studies that can guide decision-making.

96 Oleson et al. (2018) already noted the need of a global dataset on urban weather observations to  
97 properly bias-correct simulated urban climates: we here propose to use the densifying network of  
98 PWS to bias-correct urban climate simulations for urban climate impact studies. Common practice  
99 in bias-correction of urban climate simulations is to apply a single correction by the mean bias at  
100 official weather stations' rural sites, thereby assuming that the urban heat island phenomenon is  
101 accurately represented by the UCM (e.g., Lauwaet et al. (2015), or Oleson et al. (2018)). Some  
102 studies however tried considering the urban effect by linearly transforming the bias-correction  
103 coefficient via an urbanization ratio calculated at each grid cell, like in Wouters et al. (2017)  
104 over Belgium. Assuming that urban climate simulations biases cannot be linearly related to the  
105 urban fraction only, we decided to test whether urban in-situ observations can be used to perform  
106 an urban-specific bias-correction of air temperatures driven by machine learning. We hereby  
107 hypothesize that such innovative bias-correction method would be beneficial for urban heat impact  
108 studies by improving the UCM outputs on which they rely. Such innovations are needed to better  
109 assess the heat burden in cities (Nazarian et al. 2022).

110 To respond to these questions through the scope of urban near-surface temperatures, we: i)  
111 evaluated the ability of the complex three-dimensional UCM embedded in WRF – the Building  
112 Effect Parameterization coupled with its Building Energy Model (BEP-BEM) – to accurately  
113 represent the urban impact on air temperatures under two boundary layer schemes for the summer  
114 2018 in south-east England using official weather stations and PWS separately to show their added  
115 value for detecting spatially heterogeneous urban temperature biases; ii) used machine learning  
116 regressions to predict the models' daily air temperature biases in the urban environment and bias-  
117 correct the two simulations suggested in part i – which allowed us to determine an optimal time-step

118 at which the bias-correction should be performed to optimize the outputs.; and iii) compared the two  
119 bias-corrected products against the predicted daily air temperatures using only PWS measurements  
120 to investigate how realistic the bias-corrected products are. In parallel, to illustrate the benefit  
121 gained from the bias-correction for impact studies, we showcase how the bias-correction leads to  
122 different population weighted temperatures in the Greater London area.

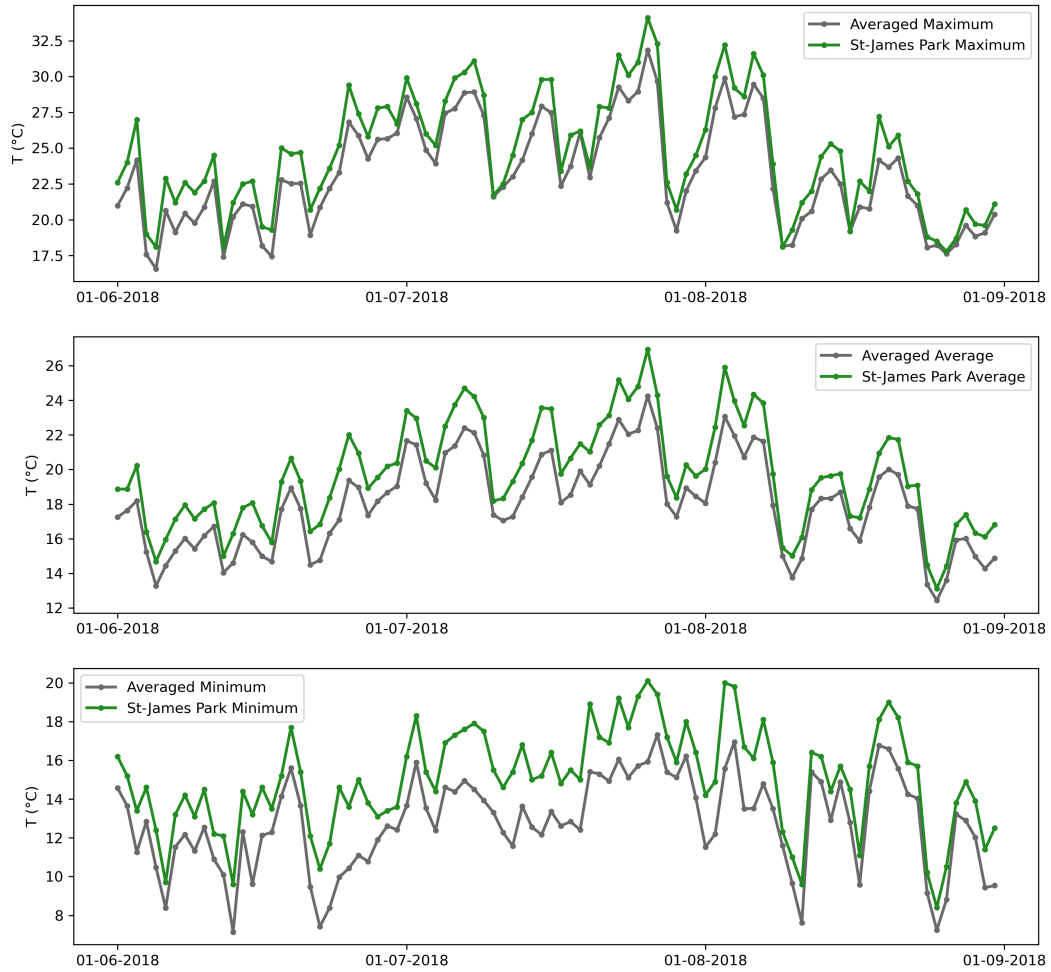
123 It is important to consider that our study does not try to estimate how a bias-corrected modelled  
124 product is better compared to a predicted product from observations for urban climate impact  
125 studies. We hereby simply try to demonstrate that any urban climate impact work that is based on  
126 urban climate modelling should pursue a spatially explicit bias-correction specific to urban areas.

## 127 **2. Methods**

### 128 *a. Model setup and region of interest*

129 We focused our study on the south-eastern parts of England, centred over the metropolis of  
130 London, host to approximately 9 million inhabitants. We chose to model the impact of urbanization  
131 on 2 m air temperature in London during the Summer of 2018, since it was one of the hottest  
132 summers in recent years. Indeed, the British Isles heatwaves of summer 2018 is considered to  
133 be the hottest summer on record for mean temperature (McCarthy et al. 2019), with maximum  
134 daily temperatures often over-passing 30 °C (Figure 2). Record temperatures, recently over-passed  
135 during the 2019 and 2022 summers, were recorded on the 26<sup>th</sup> of July with a maximum of 34.4 °C  
136 measured at London's Heathrow airport.

140 To model the impact of the urban areas of London and south-east England on local meteorology,  
141 we used the Weather Research Forecast (WRF) regional climate model version 4.3 and activate  
142 the embedded Building Effect Parameterization (BEP; Martilli et al. (2002)) urban climate model  
143 with its partner Building Energy Model (BEM; Salamanca et al. (2010); Salamanca and Martilli  
144 (2010)) – hereafter referred to as BEP-BEM. We ran the model at a horizontal resolution of 1 x  
145 1 km following a two-way nesting strategy where the outer domain is forced by ERA5 6-hourly  
146 data at 25 km with 199 by 199 grid points and the two intermediate domains are run at horizontal  
147 resolutions of 9 and 3 kilometres with 252 by 241 and 210 by 180 grid points, respectively (Figure 2,  
148 upper panel). Initial land surface conditions were provided by the default MODIS 5-arc-second  
149 land use dataset provided by the WRF community while sea surface temperatures were updated



137 FIG. 1. Daily minimum, average and maximum temperatures observed by the Met Office MIDAS automatic  
 138 weather stations. The urban St-James' Park station in central London (green) is always hotter than the average  
 139 temperature of all MIDAS stations in south-east England (grey)

150 6-hourly out of ERA-5. We ran the model in parallel over 200 CPUs using restarts every four days  
 151 of simulation. We started the simulations on the 25<sup>th</sup> of May 2018 and end them on the 31<sup>st</sup> of  
 152 August 2018, considering the first 7 days of simulation as spin-up time.

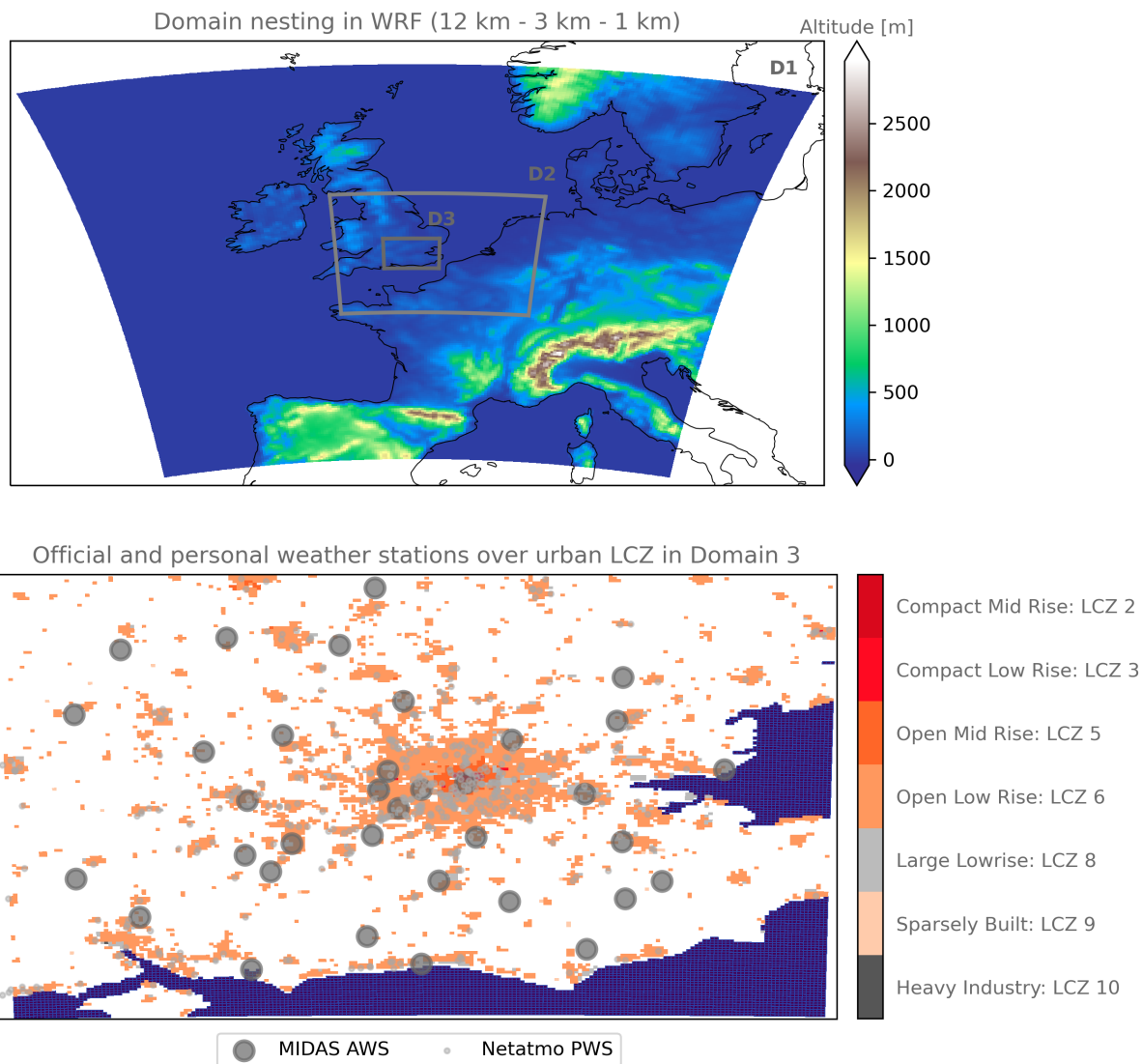
153 All domains used the same physical and dynamical parameterizations which we obtained out  
154 of preliminary testing done over the two hottest days of the summer 2018 – 26<sup>th</sup> and 27<sup>th</sup> of July  
155 2018 (see Supplements S1). We thereby used the WRF Single–moment 3–class microphysics  
156 scheme (Hong et al. 2004), the Dudhia shortwave and RRTM longwave schemes (Dudhia 1989;  
157 Mlawer et al. 1997), and the revised MM5 surface layer scheme (Jiménez et al. 2012). In the first  
158 domain, the Kain–Fritsch convection scheme was activated (Kain 2004) and then turned off in the  
159 second and third domains, which were at convection-permitting scales. We set the model top at  
160 50 hPa with an additional 5000 m damping layer and subdivided the atmosphere into 56 vertical  
161 layers. We used the Noah-MP land surface scheme (Niu et al. 2011; Yang et al. 2011) in its default  
162 parameterization over 4 soil layers.

165 Urban canopy parameters required by the WRF BEP-BEM model were provided via the newly  
166 standardized WUDAPT-TO-WRF (W2W) python package developed by Demuzere et al. (2021),  
167 following the Fortran version used by Brousse et al. (2016). This allowed the transfer of spatially-  
168 explicit morphological urban canopy parameters suitable for urban climate simulations via Local  
169 Climate Zones (LCZ) maps covering the inner domain (Figure 2, lower panel). We use the  
170 European LCZ map by Demuzere et al. (2019). Thermal and radiative parameters are also directly  
171 derived from the LCZ classification and follow those used by Stewart et al. (2014), who used these  
172 parameters for the city of Basel, Switzerland. Each parameter for roofs, walls and roads is related  
173 to each modal LCZ of the 1 km grid cell via the `URBPARAM_LCZ.TBL` (see Table 1). We decided  
174 to keep the roughness length for momentum and the lower boundary for temperatures of roofs,  
175 walls, and roads identical across each LCZ. We fixed the roughness length at 1.00E-4 m for walls  
176 and at 0.01 m for roofs and roads, respectively. For the boundary temperatures, we set it at 299 K  
177 for the roofs and the walls, respectively, and at 293 K for the road. We chose to deactivate the  
178 air conditioning in our simulation because air conditioning systems are not common in residential  
179 areas across London and surrounding cities, which compose the major part of the land use land  
180 cover.

188 In this study, two potential planetary boundary layers (PBL) schemes are compared in terms  
189 of performance and need of bias correction: the commonly used Bougeault-Lacarrère scheme  
190 (BouLac; Bougeault and Lacarrere (1989)) for urban simulations that use BEP-BEM, and the  
191 recently coupled YSU scheme to BEP-BEM (Hong et al. 2006; Hong and Kim 2008; Hendricks

163 **TABLE 1. Thermal and radiative parameters per LCZ based on Stewart et al. (2014). Road parameters are considering a mixture of asphalted and**  
 164 **concrete road pavements and grass.**

	Heat capacity [ $J \cdot m^{-3} \cdot K^{-1}$ ]			Thermal conductivity [ $J \cdot m^{-1} \cdot s^{-1} \cdot K^{-1}$ ]			Albedo			Emissivity		
	Roof	Wall	Road	Roof	Wall	Road	Roof	Wall	Road	Roof	Wall	Road
LCZ 1	1.80E+06	1.80E+06	1.75E+06	1.25	1.09	0.77	0.13	0.25	0.15	0.91	0.90	0.95
LCZ 2	1.80E+06	2.67E+06	1.65E+06	1.25	1.50	0.73	0.18	0.20	0.16	0.91	0.90	0.95
LCZ 3	1.44E+06	2.05E+06	1.63E+06	1.00	1.25	0.69	0.15	0.20	0.18	0.91	0.90	0.95
LCZ 4	1.80E+06	2.00E+06	1.54E+06	1.25	1.45	0.60	0.13	0.20	0.20	0.91	0.90	0.95
LCZ 5	1.80E+06	2.00E+06	1.50E+06	1.25	1.45	0.62	0.13	0.25	0.20	0.91	0.90	0.95
LCZ 6	1.44E+06	2.05E+06	1.47E+06	1.00	1.25	0.60	0.13	0.25	0.21	0.91	0.90	0.95
LCZ 7	2.00E+06	7.20E+05	1.38E+06	2.00	0.50	0.51	0.15	0.20	0.24	0.28	0.90	0.92
LCZ 8	1.80E+06	1.80E+06	1.80E+06	1.25	1.25	0.80	0.18	0.25	0.17	0.91	0.90	0.95
LCZ 9	1.44E+06	2.56E+06	1.37E+06	1.00	1.00	0.55	0.13	0.25	0.23	0.91	0.90	0.95
LCZ 10	2.00E+06	1.69E+06	1.49E+06	2.00	1.33	0.61	0.10	0.20	0.21	0.91	0.90	0.95



181 FIG. 2. Domain nesting (upper) and urban land cover in the inner domain (lower). The WRF nesting strategy  
 182 consists of three nested domains at 12 km (D1), 3 km (D2) and 1 km (D3) horizontal resolution. The altitude is  
 183 plotted to highlight the flat terrain of south-east England covered in D3. In the lower panel, the resulting urban  
 184 landcover in D3 after using the WUDAPT-TO-WRF python tool is presented in the form of Local Climate Zones  
 185 (LCZ). The MIDAS official automatic weather stations (AWS) and the Netatmo personal weather stations (PWS)  
 186 used for the evaluation of the model and the subsequent bias-correction using PWS only are overlaid in grey.  
 187 The sea is shown in blue in the lower panel while coastlines are drawn in black in the upper panel.

192 et al. 2020). Although we found that the latter performed better over the two hottest days of  
 193 summer 2018 (see Appendix A), we decided to keep a simulation with BouLac as YSU has only

194 been applied over Dallas (Wang and Hu 2021) whereas BouLac has been used in multiple studies  
195 already (e.g., Salamanca et al. (2011), Salamanca et al. (2012), Gutiérrez et al. (2015), Tewari  
196 et al. (2017), Mughal et al. (2019)). The Mellor-Yamada-Janjic (MYJ; Janjić (1994), Janić (2001))  
197 scheme, also available for BEP-BEM simulations, is disregarded in this study since this PBL  
198 scheme is especially used for mountainous terrain (Zonato et al. 2022), and we are modelling the  
199 relatively flat terrain of south-east England.

#### 200 *b. Model evaluation*

201 We evaluate the model’s performances against 35 official weather stations’ measurements of air  
202 temperature at 2 m obtained from the UK Met Office MIDAS network (Sunter (2021), UKMO  
203 (2021); Figure 1, lower panel). To address the issue of lack of official observations amongst the  
204 urban environment, we use Netatmo PWS to complement the model evaluation (Figure 1, lower  
205 panel). Prior to the evaluation, unrealistic PWS measurements were filtered out using the Crowd-  
206 QC v1.0 R package from Grassmann et al. (2018); details of the method can be found in Napoly  
207 et al. (2018) and other publications such as Brousse et al. (2022), who used the same dataset over  
208 London. This resulted in 407 urban PWS suitable for evaluating the UCM. Each model simulation  
209 is evaluated using a set of common statistical indicators: the root mean squared error (RMSE),  
210 the mean absolute error (MAE), the mean bias error (MB), Spearman’s coefficient of correlation  
211 ( $r$ ) and the square of Pearson’s coefficient of correlation ( $r^2$ ). These metrics are obtained using  
212 the Python scikit-learn and scipy’s stats packages from Pedregosa et al. (2011) and Virtanen et al.  
213 (2020).

#### 214 *c. Bias correction using personal Netatmo weather stations*

215 We expect urban climate simulations to have systematic biases that can be induced for a variety of  
216 reasons, such as: urban canopy parameters (Demuzere et al. 2017; Hammerberg et al. 2018; Zonato  
217 et al. 2020); complexity of urban climate models (Grimmond et al. 2011; Loridan and Grimmond  
218 2012; Lipson et al. 2021); time at which the simulation is initialised (Bassett et al. 2020); choice  
219 of initial and boundary conditions for lateral and vertical forcing (Brisson et al. 2015); or choice  
220 of model parameterizations – such as the two evaluated in this work. Hence, UCM will always  
221 present a certain degree of uncertainty that has to be coped with prior to performing urban climate

222 impact studies that use climatic variables derived from modelled simulations to estimate the impact  
223 of the urban climate on other events (e.g. mortality, biodiversity, etc.). In our study, we decided to  
224 use machine learning regressors and benefit from the high density of PWS in south-east England to  
225 correct the air temperature biases and make the simulations usable for urban heat impact studies.  
226 To our knowledge, such technique has never proposed as a viable approach for bias-correction of  
227 urban climate simulations, probably because of the lack of observations in urban areas.

228 Indeed, the practice of bias correction is to find a transformation between modelled variables  
229 and measured variables. Common practices include adding the mean bias to the modelled variable  
230 distribution or applying a separate correction to each quantile of the distribution (Maraun and  
231 Widmann 2018). Typically, observations are available only from official weather stations, which  
232 may not capture spatial variation within an urban area. Here, because we want to use observations  
233 which represent the spatial variation within urban areas at the 1 km scale, we developed an  
234 innovative method for bias-correction. Using regression, we predict the bias in the modelled air  
235 temperature at 2 m ( $T_2$ ) relative to the PWS observations at each model grid cell which has PWS  
236 observations. This prediction is based on the same set of spatially explicit morphological urban  
237 canopy parameters at 1 km horizontal resolution that were inputs to the UCM. These include the  
238 urban fraction, the surface height, the average building height, the building surface to plan area  
239 fraction ( $\lambda_b$ ), the plan area fraction ( $\lambda_p$ ) and the frontal area fraction ( $\lambda_f$ ). We are therefore making  
240 the assumption that the spatial variation in the bias of the model is dependent only upon its spatial  
241 inputs.

242 We chose to bias-correct the simulated daily minimum, maximum and average  $T_2$  ( $T_{2min}$ ,  $T_{2max}$ ,  
243 and  $T_{2mean}$ ) using filtered PWS observations in London and south-east England. To do so, only  
244 PWS that have less than 4 hours per day without data and that are located in urban pixels with  
245 an urban fraction greater than 0 are retained – where the WRF land-use land-cover at 1 km  
246 horizontal resolution refers to an LCZ. Daily temporal scale is considered optimal as it combines  
247 a higher spatial density of measurements compared to hourly data and a lower computational  
248 requirement; it is also a commonly used temporal scale for urban heat impact studies. Daily  
249 minimum and maximum air temperatures at 2 m are defined following the Met Office Had-UK  
250 definition: minimum temperature observed from 9AM of the previous day d-1 to 9AM of the d

TABLE 2. Hyperparameter tuning used by each regressors

Model	Parameters Dictionary
Linear	'normalize': False
Ridge	'alpha': 1, 'normalize': True, 'random_state': 42, 'solver': 'lsqr', 'tol': 0.01
Lasso	'alpha': 1, 'normalize': False, 'random_state': 42, 'selection': 'random', 'tol': 1e-10
Random Forest	'max_features': 'sqrt', 'min_samples_leaf': 11, 'min_samples_split': 2, 'n_estimators': 400, 'random_state': 42
Gradient Boosting	'learning_rate': 0.2, 'max_depth': 3, 'max_features': 'sqrt', 'min_samples_leaf': 10, 'min_samples_split': 22, 'n_estimators': 200, 'random_state': 42, 'subsample': 0.2

251 day, and maximum temperature observed from 9AM of the  $d$  day to 9AM of the next day  $d+1$   
 252 (Hollis et al. 2019).

253 We test the ability of 6 different regressors of increasing complexity available in the Python  
 254 scikit-learn packages (Pedregosa et al. 2011) to predict the model bias based on WRF spatial  
 255 urban canopy parameters only. These regressors are: dummy regression (which simply returns  
 256 the mean), linear regression, Ridge regression, Lasso regression, Random Forest regression, and  
 257 Gradient Boosting regression. Each of the different regressors, except the dummy regression,  
 258 offers a set of parameters that can be fine-tuned to increase each regressor's performance. Hence,  
 259 prior to running the daily bias-correction we use a 5 K-fold cross-validation using the Grid Search  
 260 CV package from scikit-learn in Python to evaluate the impact of hyperparameter tuning on the  
 261 regressors' performances based on RMSE, MAE and  $r^2$ . The cross-validation is done over the  
 262 summertime average daily mean temperature bias from the control run only, for computational  
 263 reasons. We retain RMSE as the refitting score to better capture the spatial spread and extremes of  
 264 T2. The resulting parameterizations are given in Table2. We chose to keep the same hyperparameter  
 265 tuning for all bias correction and predictions to ease comparability between the outcomes.

266 Once the hyperparameter tuning is done and prior to performing the final bias-correction, we  
 267 test if the bias-correction is beneficial for palliating to the models' bias and if it also benefits from  
 268 training the regressors at the daily time-step or if a training using the time-mean bias is sufficient.  
 269 To perform this evaluation using the same metrics as in the model evaluation, we bootstrap each  
 270 regressors 25 times, randomly sampling 80 % of the data as training and the remaining 20 %  
 271 as testing – for both the daily-minimum, -maximum and -average, and their respective summer  
 272 time-mean average. The average predicted daily T2\_BC of all predicted T2\_BC in the test sample  
 273 is then compared against the observed T2 – for daily-minimum, -maximum and -average.

274 After this final step, we bias-correct both the BouLac and the YSU runs using 100 % of the  
275 PWS data to compare the spatial outcomes. We also predict T2 out of PWS' observed T2 with the  
276 same set of covariates used to predict the model bias to illustrate how divergent each bias-corrected  
277 model outputs are to a simplified predicted T2 that is not a derivative of any model constraint.  
278 Because more refined and complex techniques exist to predict air temperature from PWS and very  
279 high-resolution earth observations (e.g., Venter et al. (2020), Venter et al. (2021)), we do not  
280 evaluate these predicted temperatures which should simply be considered as an illustration of how  
281 bias-corrected products are similar or divergent to observational data.

282 Lastly, to illustrate the potential benefit of modelled air temperature bias-correction prior to  
283 urban heat impact studies, we calculate the average population weighted temperatures – based on  
284 the United Kingdom census data from 2011 – in Greater London before and after the bias-correction.

### 285 **3. Results**

#### 286 *a. WRF simulation evaluation*

287 When we evaluate the two model simulations against MIDAS official weather stations only, they  
288 perform similarly, demonstrating a systematic negative bias of  $\sim 0.55$  °C on average (Table 3). The  
289 average correlation with the automatic weather stations following the squared Pearson's  $r^2$  is of  
290 0.77 for BouLac and 0.79 for YSU, while using Spearman's  $r$  it is of 0.86 and 0.88, respectively. A  
291 slight decreased performance is found in urban pixels for YSU, with an average MAE of 1.83 °C  
292 and a negative MB of 0.79 °C compared to BouLac's 1.82 °C for MAR and -0.56 °C for MB.  
293 In general, the bias is more important at night, and, in non-urban stations, performances are  
294 similar. Hence, looking only at the models' performances using standard in-situ observations  
295 doesn't provide information on which model represents the urban climate more accurately.

306 On the other hand, comparison with PWS observations identifies differences in performance in  
307 urban areas between the models, as shown by the performance metrics plotted in Figure 3 and B1.  
308 The BouLac simulation has a stronger cool bias of  $-1.46$  °C  $\pm$   $0.6$  °C on average in the urban area,  
309 compared to YSU's MB of  $-0.99$  °C  $\pm$   $0.82$  °C. RMSE and MAE are similar, with values of  $2.79$  °C  
310  $\pm$   $0.36$  °C and  $2.20$  °C  $\pm$   $0.32$  °C for BouLac and  $2.66$  °C  $\pm$   $0.40$  °C and  $2.15$  °C  $\pm$   $0.35$  °C for  
311 YSU. These metrics are consistent with the MIDAS observations, highlighting a systematic cool  
312 bias of the model and a coefficient of determination ( $r^2$ ) of 80 %. Importantly, the variability in

296 TABLE 3. Average of all performance metrics calculated at each MIDAS official weather stations for hourly air  
 297 temperature at 2 m for the summer period (1<sup>st</sup> June 2018 to the 31<sup>st</sup> of August 2018). Urban stations are stations  
 298 located in a pixel classified as an urban LCZ in WRF and rural stations are located in other natural land-use  
 299 land-cover.

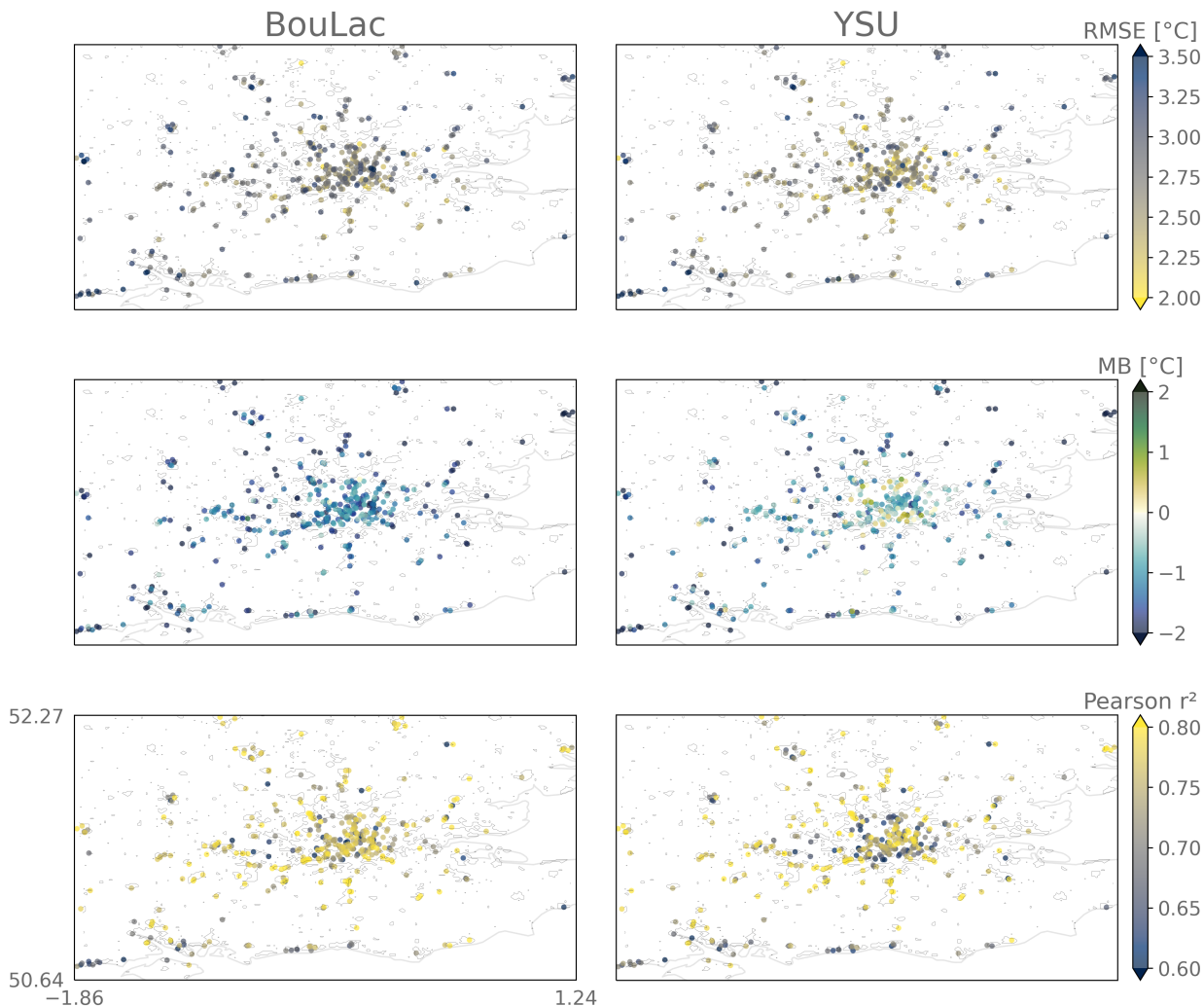
	BouLac					YSU				
	RMSE	MAE	MB	r <sup>2</sup>	r	RMSE	MAE	MB	r <sup>2</sup>	r
<b>All</b>	2.33	1.82	-0.56	0.77	0.86	2.31	1.83	-0.57	0.79	0.88
<b>Urban</b>	2.42	1.88	-0.73	0.76	0.86	2.42	1.92	-0.93	0.77	0.87
<b>Rural</b>	2.32	1.81	-0.53	0.78	0.86	2.28	1.81	-0.50	0.80	0.88

313 the model’s performance is more greater in the YSU run – reflected by greater standard deviations  
 314 of performance metrics – and, in the BouLac simulation, the metrics are more heterogeneously  
 315 distributed amongst the urban area. Indeed, when we look at the YSU simulation, we can see  
 316 that the model has a smaller MB in suburban areas and a greater MB in the city centre. Yet, in  
 317 parallel, the correlation with the PWS is lower in the suburban areas and higher in the centre of the  
 318 city. This could mean that YSU accurately represents the urban temperatures on average due to  
 319 compensating effects, which we do not intend to evaluate in this study. Nevertheless, this shows  
 320 how PWS are beneficial for capturing the spatial heterogeneity of each model’s performance and  
 321 therefore supports the use of spatially-varying bias-correction.

322 *b. Bias correction of urban climate simulations*

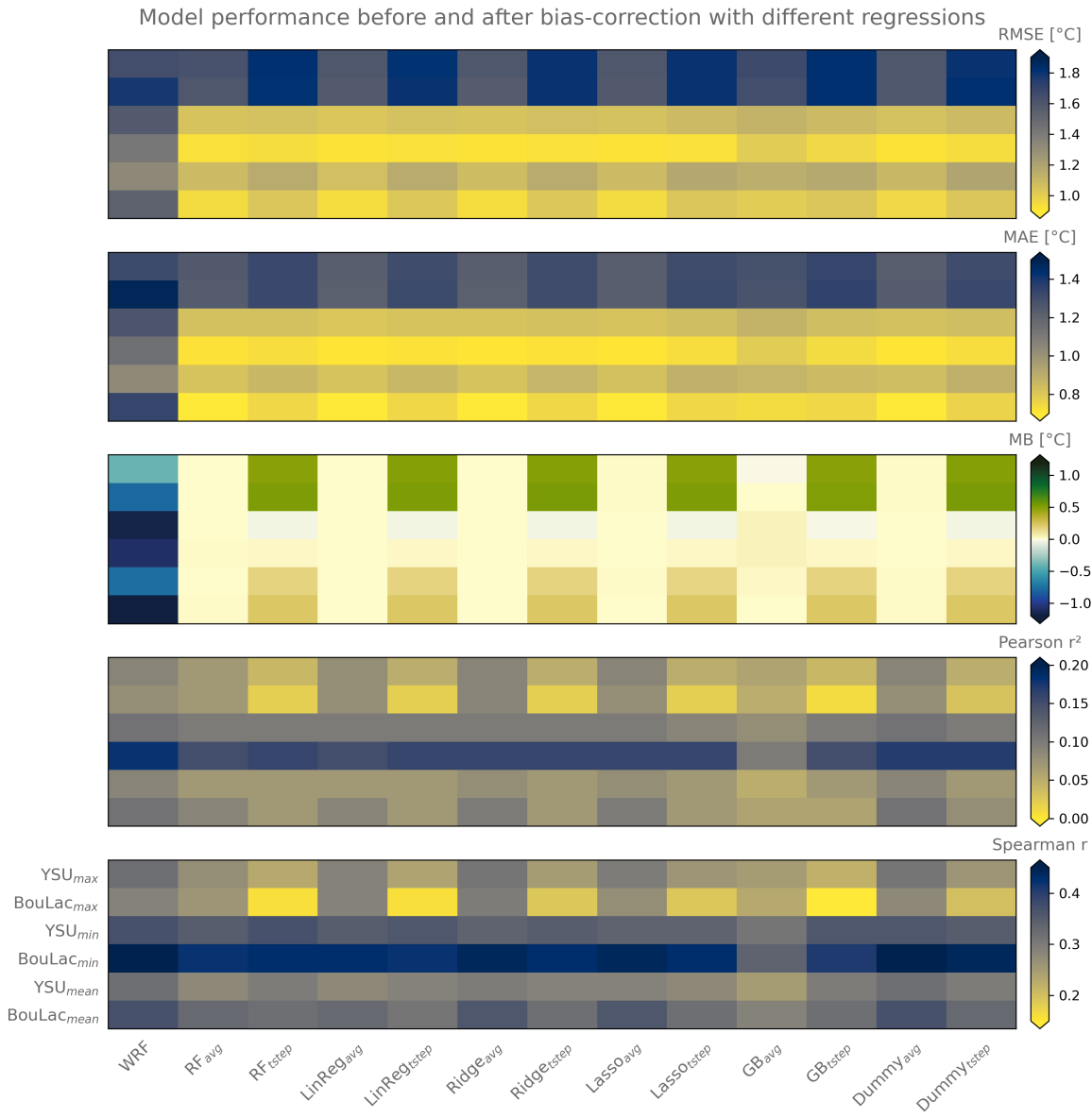
323 Over our domain of study covering south-east England during the Summer 2018, both models  
 324 are subject to a cold negative bias of  $\sim -0.5$  °C on average according to official stations and of  
 325  $\sim -1.0$  °C to  $\sim -1.5$  °C according to PWS. But as demonstrated above, the bias of the models against  
 326 PWS observations has substantial spatial variation and so the bias correction for urban heat impact  
 327 studies should be spatially explicit.

333 After performing a bootstrapping procedure – running the bias-correction 25 times with 80 %  
 334 of the CWS as training data and 20 % as testing samples – we can see that each machine learning  
 335 regressors give similar performance(Figure 4; values numerically given in Tables B1 and B2 ). All  
 336 bias-corrections were however beneficial compared to the original outputs from the WRF model,  
 337 reducing RMSE, MAE and MB by 0.29 °C, 0.32 °C and 1.02 °C on average. The bias-correction  
 338 was most efficient for daily-minimum temperatures and less for daily-maximum temperatures,



300 FIG. 3. Performance metrics calculated at location of each citizen personal weather station (PWS) for the  
 301 two model simulations using different planetary boundary layer schemes (YSU and BouLac). The metrics are  
 302 calculated over the whole summer 2018 with hourly outputs of near surface air temperature at 2 m. Root  
 303 mean square error (RMSE) and mean bias (MB) are given in degrees Celsius ( $^{\circ}\text{C}$ ). Coefficients of correlation  
 304 measured with the squared Pearson's  $r$  are also provided. Mean absolute error (MAE) and Spearman's  $r$  are given  
 305 in Figure B1 to increase clarity.

339 where RMSE was not diminished – if not slightly increased (by  $0.05\text{ }^{\circ}\text{C}$  for YSU daily-maximum  
 340 temperatures for example) – by the time-step bias-correction. Interestingly, the spatial correlation  
 341 between the bias-corrected and the observed temperatures are low, with values ranging from around

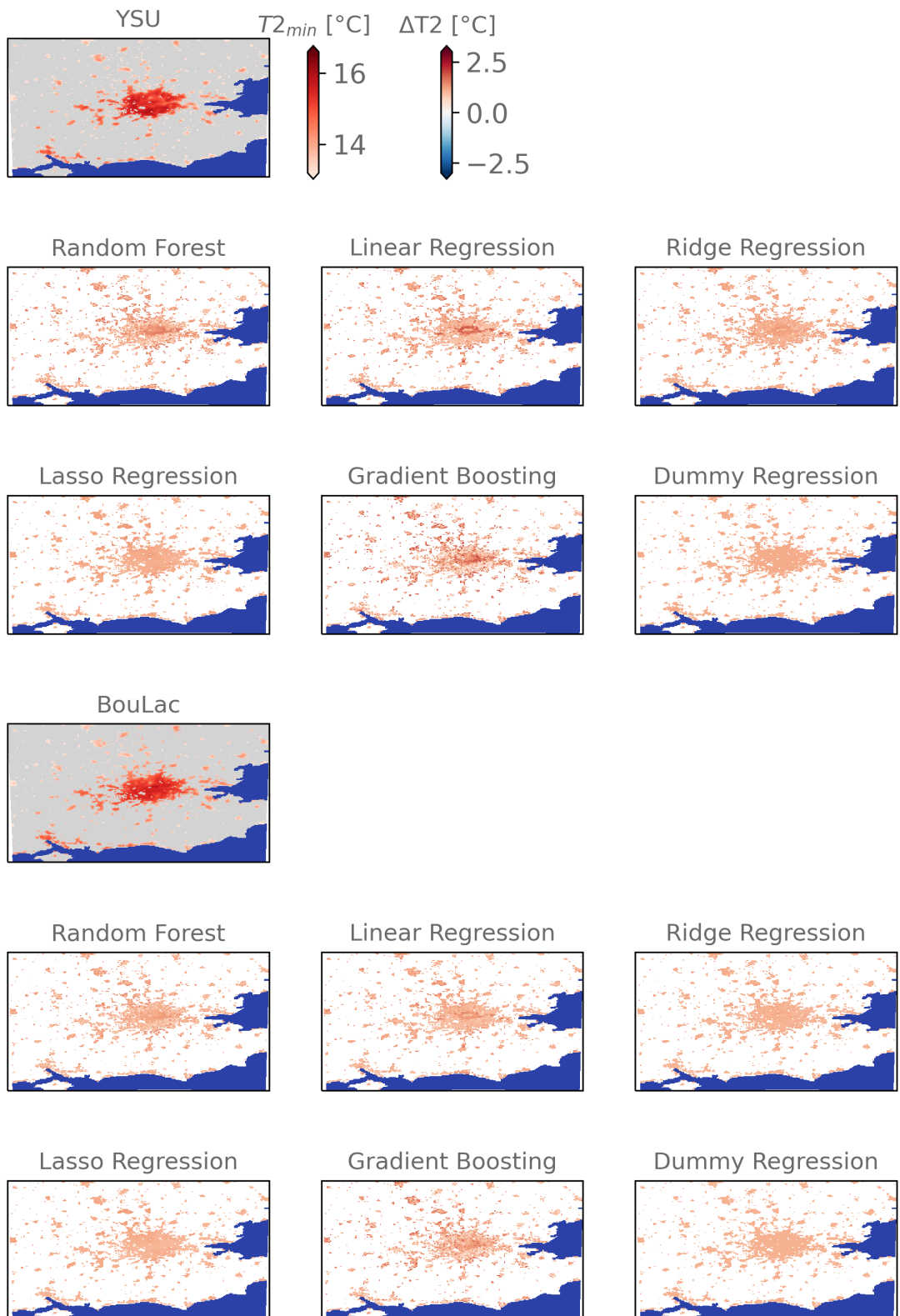


328 FIG. 4. Performance metrics for the model prior to the bias-correction (WRF) and all the different regressions  
 329 (random forest: RF; linear regression: LinReg; Ridge regression: Ridge; Lasso regression: Lasso; gradient  
 330 boosting: GB; and dummy regression: Dummy). The different regressions are assigned a suffix: “avg”  
 331 for regressions that were trained on the summer time-mean average of daily-minimum, -mean or -maximum  
 332 temperatures, and “tstep” for those that were trained with the temperatures at each daily time-step.

342 0.02 to 0.2 for the squared Pearson's  $r$  and from around 0.15 to 0.45 for Spearman's  $r$ . This can  
343 be expected as machine learning algorithms have difficulties representing a time-varying variable  
344 with static spatial elements only (Georganos et al. 2021; Venter et al. 2021). Unexpectedly, we find  
345 that the training at the daily time-step does not outperform the training at the summer time-mean  
346 in terms of spatial correlation with the heat distribution across London. Nonetheless, if we take  
347 the average daily-minimum, -mean and -maximum temperatures of all CWS and compare it to  
348 the modelled temperatures, we find that the time-step bias-correction is closer to the observations  
349 (Figures B2 to B4).

350 Comparing the spatial differences of the bias-corrected products related to the complexities of  
351 each regressors, we find that although each regressor is performing similarly on average, important  
352 disparities are found between the outputs. For example, when looking at the average bias-correction  
353 imposed to daily-minimum temperatures after training the regressors at each time-step, the Lasso  
354 and the Ridge regressors impose a flat bias-correction, similar to the dummy regression, while the  
355 random forest and gradient boosting regressors' degrees of freedom result in a spatially diverse  
356 bias-correction (Figure 5 and Figures B5 and B6). Besides, the linear regression imposes an average  
357 bias-correction spatially-correlated to the modal LCZ. In general, the signal is consistent across  
358 each regressors, apart from the Lasso and the dummy regression, where, for YSU, central London  
359 requires a stronger bias-correction by 1 °C to 2 °C compared to the suburban areas where the  
360 bias-correction is around 0.5 °C ; for BouLac, the central bias-correction is lower than YSU. We  
361 find that these spatial tendencies are also found for daily-maximum and daily-average temperatures,  
362 defending our hypothesis of a systematic bias correlated to spatially explicit input parameters. The  
363 spatial differences in bias-correction are however less important for daily-maximum temperatures,  
364 which is the time at which the urban heat island is also expected to be the lowest.

Modelled temperatures and respective bias-corrections with multiple regressors



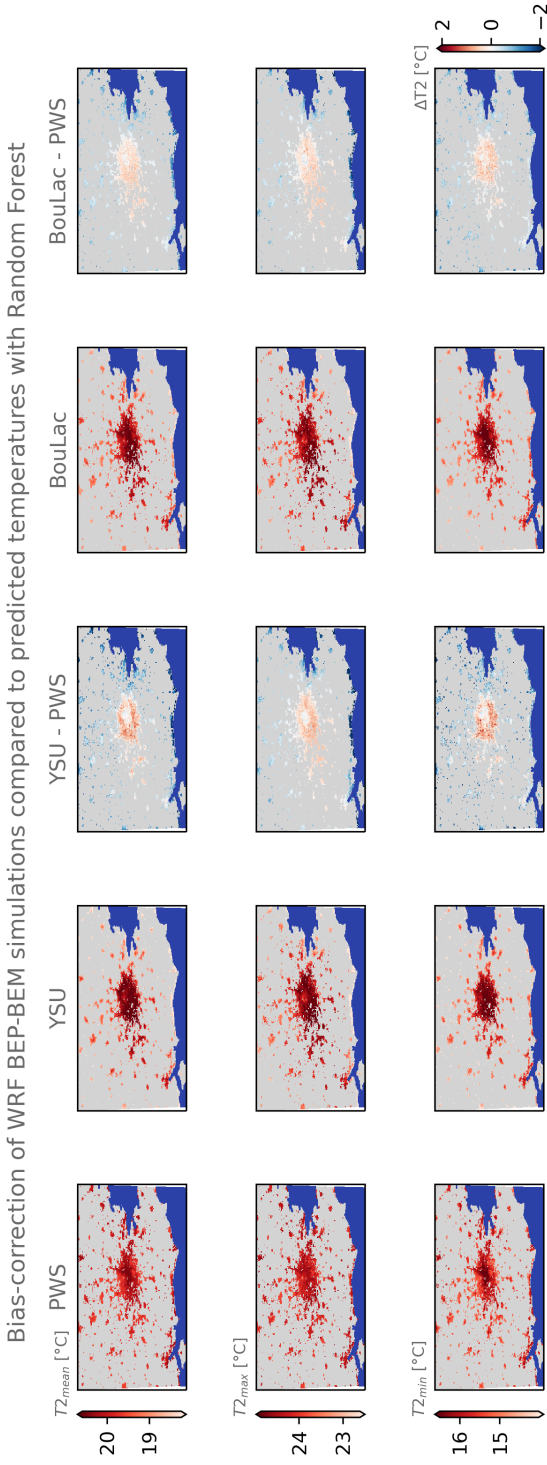
365 FIG. 5. All regressions propose different bias-corrections ( $\Delta T_2$ ) of the average modelled absolute daily  
366 minimum urban temperature ( $T_{2_{min}}$ ). Differences of bias-correction are observed between the runs with different  
367 planetary boundary layer schemes (Bougeault-Lacarrère – BouLac, and Yonsei University – YSU). The centre  
368 of London is subject to a stronger bias-correction. Rural lands are masked in grey and the seas in blue. Bias  
369 corrections of daily mean and maximum temperatures are given in Figures B5 and B6

370 Finally, we find that the bias-corrected BouLac simulation corresponds spatially to predicted  
371 temperatures using PWS more than YSU – something we find equally across all regressors (Figure 6  
372 and Figures B7 to B11). As an example, when comparing the average bias-corrected products  
373 using the time-step trained random forest regressor we can see that YSU urban heat is more  
374 homogeneously distributed than BouLac’s or the predicted temperatures from PWS only. BouLac’s  
375 bias-corrected product shows stronger urban heat in central London compared to suburban areas,  
376 coherent with the predicted temperatures. Nonetheless, BouLac’s suburban areas are hotter by  
377 0.5 °C to 1.0 °C than the predicted ones with PWS only. This remains less pronounced than in  
378 YSU. Lastly, we can see that both bias-corrected products show similar trends when compared  
379 to the PWS-only predicted temperatures with hotter suburban areas and cooler secondary cities  
380 as well as coastlines. Again, this does not show which product between the PWS-only predicted  
381 temperatures and the bias-corrected products is better since we do not evaluate this here.

382 These results show that bias-correction of modelled air temperature change their spatio-temporal  
383 distributions. When focusing on the potential impact bias-correction may have in estimated urban  
384 heat impact on urban health, we find that using the random forest regression trained at each daily  
385 time-step leads to an increased average population weighted temperature by 0.77 °C in the YSU  
386 case, and of 1.24 °C in the BouLac case. Raw model outputs are thereby lowering the impact of  
387 heat on the urban population.

#### 394 4. Discussion and conclusions

395 In this study, we argue that the joint use of crowd-sourced personal weather stations (PWS) and  
396 urban climate models (UCMs) can add value to urban climate research and in particular to urban  
397 climate impact research. This is supported by two major outcomes of our case-study focused over  
398 London during the summer 2018. First, we showed that evaluation of urban climate simulations  
399 using PWS enables the detection of spatially-varying systematic biases in urban areas related to the



382 Fig. 6. The random forest regressor leads to different bias-corrections of the two WRF simulations parameterized with different turbulence schemes  
 383 – the Yonsei University (YSU) and the Bougeault-Lacarrère (BouLac) – and with the BEP-BEM urban canopy model activated. This holds for average  
 384 daily mean, minimum and maximum temperatures ( $T_{2_{mean}}$ ,  $T_{2_{min}}$  and  $T_{2_{max}}$ ) after the daily time-step bias-correction. Compared to the predicted  
 385 temperatures using the personal weather stations data only (PWS), the bias-corrected products are hotter in the suburban areas of the Greater London and  
 386 cooler in the rural areas. The difference is more pronounced in YSU (see YSU – PWS). Greyed areas represent natural areas where the bias-correction  
 387 is not performed and the sea is shown in dark blue. The same figures for the other regressors are given in Figures B7 to B11

400 UCMs’ parameterization, which are not detectable using only official weather stations. Second,  
401 we demonstrated that PWS, combined with detailed morphological data derived from LCZ maps,  
402 can be used to derive a spatially varying bias-correction via commonly used machine-learning  
403 regressors. This latter point has major implications for urban climate impact research – and  
404 especially future urban climate impact studies – as we hereby propose the first bias-correction  
405 technique that considers the existence of a non-linear spatially heterogeneous bias in modelled  
406 urban climates.

407 Of course, using PWS for evaluating UCM simulations should always cautiously be considered  
408 because of the lower accuracy of PWS and the potential uncertainties related to user-driven mistakes  
409 in the set-up of their PWS (e.g., indoor sensors instead of outdoor, poor shading conditions, height  
410 of the sensor, etc.). However, reliable tools have now been developed since the first use of PWS for  
411 model evaluation by Hammerberg et al. (2018) to filter dubious measurements out (e.g., Crowd-QC  
412 from Napoly et al. (2018) or Crowd-QC + by Fenner et al. (2021)), thus making PWS observations  
413 increasingly reliable. This does not resolve the question of the representativity of measurements,  
414 i.e., “how is one PWS measurement representative of the simulated urban pixel?” Yet, the increasing  
415 density of PWS in the urban environments begins to alleviate this uncertainty. For example, Venter  
416 et al. (2020) found that a density of one PWS per square kilometre is optimal for predicting seasonal  
417 air temperature in Oslo. Dense PWS networks hence permit the detection of systematic biases  
418 that would otherwise pass undetected. Therefore, to support the development of PWS as a source  
419 of urban weather observations for model evaluation, urban climate scientists should identify an  
420 optimal density of PWS for UCM evaluation, to define which cities are in need of urban weather  
421 observations, and to start instigating common frameworks and standards.

422 We consider our study innovative and supportive of future advances in the field because it is the  
423 first bias-correction technique in urban environments which considers that UCMs’ simulated UHI is  
424 spatially heterogeneous in its accuracy and that the UHI is not solely linearly correlated to the urban  
425 fraction. Aided by the expanding fields of crowd-sourcing weather observations through PWS,  
426 machine learning, and potentially deep learning, we infer that our work should serve as the basis of  
427 future research that would try, but not restricted to, improving the bias-correction of urban climate  
428 models using PWS. For instance, we did not find any machine learning regressor to be more efficient  
429 at predicting the model bias. This could be explained by the rather restricted set of covariates we

430 used for training the regressors as well as the coarse horizontal resolution of 1 km at which the  
431 covariates were aggregated to be consistent with the model's spatial resolution. Higher spatial  
432 resolutions and more specific satellite earth observations could be used to improve regressors'  
433 performance, following up on the work by Venter et al. (2021), for example. When modelling the  
434 near-surface UHI, which is not a model bias, their regressor achieved similar performances as ours,  
435 with an RMSE of 1.05 °C and a Pearson's  $r^2$  of 0.23. Although the common use of model's input  
436 parameters and earth observations as covariates could be beneficial, a particular attention should  
437 be given to the choice of earth observations since these should not be decorrelated to the model's  
438 physics and dynamics as the purpose would remain the bias-correction.

439 Besides, as our results showed by comparing the performance of regressors trained at the daily  
440 time-step and with the summer time-mean average, regressors could gain in performance by adding  
441 a temporal component to the covariates. Following up on this idea, the recent work by (Zumwald  
442 et al. 2021) tried predicting the near-surface air temperature in Zurich for the 30<sup>th</sup> of June 2019 out  
443 of ~650 Netatmo PWS' measurements during the preceding week. Their set of covariates consisted  
444 of spatial earth observations as well as 35 meteorological predictors that were all derived from one  
445 official automatic weather stations. The latter predictors helped training the model to recognise  
446 how the temperature measured at each PWS location was related to the meteorological variables  
447 measured at the automatic weather stations. Their predictions at hourly time-steps achieved  
448 reasonable performances with RMSEs around 1.70 °C. Bias-correction of UCM simulations could  
449 hence be improved by incorporating temporally explicit meteorological observations from official  
450 weather stations. Notwithstanding, this would require extensive investigation on the area down  
451 to which each official station is representative for training the regressors. More geographically  
452 oriented machine learning regressors, like the geographical random forests (Georganos et al. 2021),  
453 could also help integrate these spatial heterogeneities for an improved bias-correction.

454 In general, we support the use of quality-controlled PWS observations for bias-correction of  
455 urban climate simulations. As shown in this case study, model outputs prior to any bias-correction  
456 could lead to under- or over-estimation of urban heat impact on public health. We indeed find  
457 that for the summer 2018 in London, average population weighted temperatures were higher  
458 after bias-correcting the model outputs, suggesting higher urban heat related mortality during this  
459 period. This simple example shows that bias-correction of urban climate simulations could have

460 important implications for calculating the exposure of urban citizen to heat or estimating the urban  
461 heat-related mortality. Although preferring bias-corrected model outputs to predicted urban air  
462 temperatures from earth observations for present-day urban heat impact studies is not covered in  
463 this study – and must be further explored – we still argue that bias-correction should be done  
464 prior to any urban heat impact studies that imply using climate model outputs. This argument  
465 is especially valid for future climate projections at urban scale and we encourage future research  
466 to investigate how to transfer present urban bias-correction coefficients to simulated future urban  
467 climates. Doing so, bias-corrected simulations could help targeting areas where heat mitigation or  
468 adaptation strategies could be more beneficial as their efficiency is dependent on their location and  
469 scales of implementation (Yang and Bou-Zeid 2019; Broadbent et al. 2022).

470 *Acknowledgments.* We personally thank Stefanos Georganos for his help and his comments on  
471 machine learning classifiers and regressors. We also thank Daniel Fenner and Fred Meier for their  
472 valuable insights concerning data acquisition, filtering and treatment of crowd-sourced citizen  
473 weather stations. Lastly, we are grateful to Matthias Demuzere and other committed members of  
474 the WUDAPT project for providing the European LCZ map and the python W2W tools. CH is  
475 supported by a NERC fellowship (NE/R01440X/1) and acknowledges funding for the HEROIC  
476 project (216035/Z/19/Z) from the Wellcome Trust, which funds OB and CS.

477 OB designed the study and led the conception of the manuscript with the support of CH and  
478 CS. OB was responsible for the WRF modelling, the model evaluation and the bias-correction.  
479 CS provided support in the python coding and in the statistical analysis for the bias-correction.  
480 OK was responsible for technical support of the installation of WRF on the University College  
481 London’s “Kathleen” and “Myriad” super-computers. AZ and AM offered guidance in the set-up  
482 of the WRF model v4.3 and urban heat modelling expertise with SK. All authors contributed to  
483 the writing of the manuscript.

484 The authors declare no conflicts of interest.

485 *Data availability statement.* The simulations done in this research were performed using the WRF  
486 model v4.3 (<https://github.com/wrf-model/WRF.git>). The related outputs presented in this  
487 research and the scripts used to produce them are available upon reasonable request addressed to  
488 the corresponding author.

**Model sensitivity testing over the two hottest days of Summer 2018**

Prior to running the 3-months simulation, we tested the model's sensitivity to a set of parameterization to assess which model is the best performing model for the 3-months simulation. We perform the sensitivity in a progressive way; parameters are kept if beneficial, removed if detrimental. We chose to run the simulations over the two hottest days of the summer 2018 with one additional day as spin-up time – from the 25<sup>th</sup> to the 27<sup>th</sup> of July 2018 – to see how the model is capable of accurately representing an extreme condition in terms of air temperature at 2 m – tested against official MIDAS automatic weather stations and personal Netatmo PWS. The model was also tested for relative humidity and wind speed at 10 m at MIDAS locations where records were available. All wind-speed measurements are converted from knots to  $\text{m}\cdot\text{s}^{-1}$ .

We start from Heaviside et al. (2015) model's parameterization, who simulated the impact of urbanization on the local climate in the West Midlands in England, but supplement the CORINE land-use land-cover by the Local Climate Zones classification instead since Brousse et al. (2016) compared both products and proved the added value of LCZ over Madrid. We chose the work by Heaviside et al. (2015) as a starting point since it also uses the BEP urban climate model, coupled to the WRF model and is one of the only WRF simulations done over England.

From there, our simulations tested: i) the use of YSU, recently coupled to the BEP-BEM model (Hendricks et al. 2020), instead of Bougeault-Lacarrere; ii) the use of the more complex land surface scheme Noah-MP in its default parameterization instead of the default Noah land surface model; iii) the forcing by ERA5 reanalysis data at 25 km horizontal resolution instead of ERA-Interim; iv) the reduction of soil moisture by 50 % and its increase by 200 %, following suggestions provided by Martilli et al. (2021). We chose not to test the impact of urban canopy parameters in this case to keep our simulations standardized and universally coherent through the LCZ scheme. Their simulation used the same micro-, clouds, convection and radiation physics than ours.

We found that all steps taken from the original parameterization by Heaviside et al. (2015) were beneficial to the model's performance. Through an intermediate simulation where we tested again the BouLac turbulence scheme after step iii, we found that YSU was still performing better.

517

## APPENDIX B

518

### Additional Figures and Tables

519

This section presents all the figures that are not given in the main text.

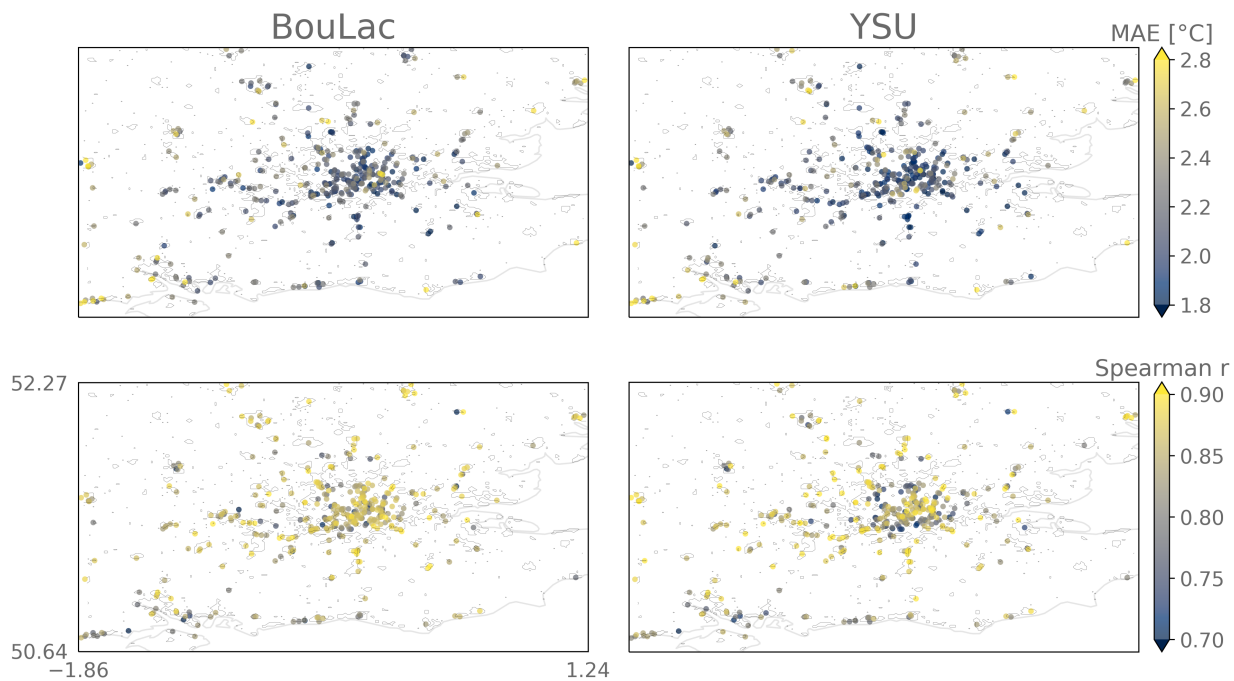


FIG. B1. Same as figure 3, but for MAE and Spearman's r.

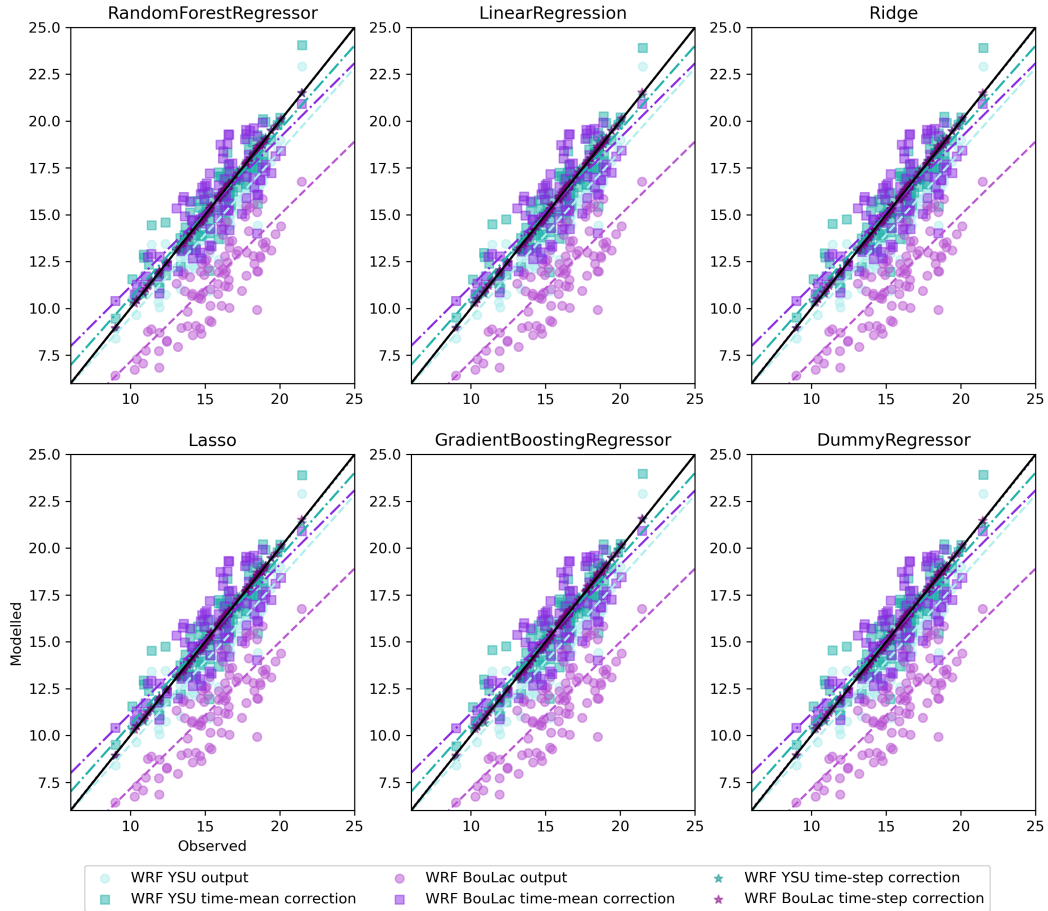
520 TABLE B1. Performance metrics used in Figure 4 for the model using BouLac prior to the bias-correction (WRF) and all the different regressors  
521 (random forest: RF; linear regression: LR; Ridge regression: RD; Lasso regression: LA; gradient boosting: GB; and dummy regression: DU). The  
522 different regressions are assigned a suffix: “avg” for regressions that were trained on the summer time-mean average of daily-minimum, -mean or  
523 -maximum temperatures, and “tstep” for those that were trained with the temperatures at each daily time-step.

	BouLac												
	WRF	RF <sub>avg</sub>	RF <sub>tstep</sub>	LR <sub>avg</sub>	LR <sub>tstep</sub>	RD <sub>avg</sub>	RD <sub>tstep</sub>	LA <sub>avg</sub>	LA <sub>tstep</sub>	GB <sub>avg</sub>	GB <sub>tstep</sub>	DU <sub>avg</sub>	DU <sub>tstep</sub>
<b>MEAN</b>													
<b>RMSE</b>	1.54	0.95	1.04	0.94	1.03	0.94	1.03	0.95	1.04	1.01	1.04	0.96	1.04
<b>MAE</b>	1.34	0.69	0.75	0.69	0.75	0.68	0.75	0.69	0.75	0.74	0.75	0.7	0.76
<b>MB</b>	-1.2	0.01	0.23	0	0.23	0	0.23	0	0.23	0	0.23	0.01	0.23
<b>Pearson r<sup>2</sup></b>	0.11	0.09	0.07	0.09	0.07	0.1	0.07	0.1	0.07	0.06	0.06	0.11	0.08
<b>Spearman r</b>	0.37	0.33	0.32	0.33	0.31	0.36	0.32	0.36	0.32	0.29	0.32	0.37	0.33 0.88
<b>MIN</b>													
<b>RMSE</b>	1.42	0.93	0.94	0.92	0.93	0.92	0.93	0.92	0.93	1.01	0.96	0.92	0.94
<b>MAE</b>	1.15	0.72	0.73	0.71	0.72	0.71	0.72	0.71	0.73	0.79	0.74	0.71	0.73
<b>MB</b>	-1.08	0.01	0.02	0	0.02	0	0.02	0	0.02	0.04	0.02	0	0.02
<b>Pearson r<sup>2</sup></b>	0.18	0.15	0.16	0.15	0.16	0.16	0.16	0.16	0.16	0.1	0.15	0.17	0.17
<b>Spearman r</b>	0.46	0.42	0.43	0.43	0.42	0.44	0.43	0.44	0.43	0.34	0.41	0.46	0.44
<b>MAX</b>													
<b>RMSE</b>	1.78	1.6	1.81	1.58	1.8	1.57	1.8	1.59	1.8	1.65	1.82	1.6	1.82
<b>MAE</b>	1.48	1.24	1.33	1.22	1.32	1.22	1.31	1.23	1.32	1.28	1.35	1.24	1.33
<b>MB</b>	-0.79	0	0.52	0	0.52	0	0.53	0.01	0.52	0	0.51	0.01	0.53
<b>Spearman r</b>	0.08	0.07	0.02	0.08	0.02	0.09	0.02	0.08	0.02	0.05	0.01	0.08	0.03
<b>Spearman r</b>	0.29	0.26	0.16	0.29	0.16	0.3	0.19	0.27	0.19	0.23	0.14	0.28	0.2

524 TABLE B2. Performance metrics used in Figure 4 for the model using YSU prior to the bias-correction (WRF) and all the different regressors (random  
525 forest: RF; linear regression: LR; Ridge regression: RD; Lasso regression: LA; gradient boosting: GB; and dummy regression: DU). The different  
526 regressions are assigned a suffix: “avg” for regressions that were trained on the summer time-mean average of daily-minimum, -mean or -maximum  
527 temperatures, and “step” for those that were trained with the temperatures at each daily time-step.

YSU		WRF	RF <sub>avg</sub>	RF <sub>step</sub>	LR <sub>avg</sub>	LR <sub>step</sub>	RD <sub>avg</sub>	RD <sub>step</sub>	LA <sub>avg</sub>	LA <sub>step</sub>	GB <sub>avg</sub>	GB <sub>step</sub>	DU <sub>avg</sub>	DU <sub>step</sub>
<b>MEAN</b>														
<b>RMSE</b>	1.33	1.09	1.16	1.07	1.16	1.08	1.16	1.09	1.18	1.15	1.17	1.1	1.19	
<b>MAE</b>	1.04	0.82	0.86	0.82	0.86	0.82	0.87	0.83	0.89	0.87	0.85	0.84	0.89	
<b>MB</b>	-0.76	0	0.17	0	0.17	0	0.17	0.01	0.16	0.02	0.17	0.01	0.17	
<b>Pearson r<sup>2</sup></b>	0.09	0.07	0.07	0.07	0.07	0.08	0.07	0.08	0.07	0.05	0.07	0.09	0.07	
<b>Spearman r</b>	0.32	0.28	0.3	0.28	0.29	0.3	0.29	0.29	0.28	0.25	0.3	0.32	0.3	
<b>MIN</b>														
<b>RMSE</b>	1.58	1.05	1.06	1.04	1.06	1.05	1.07	1.06	1.09	1.12	1.09	1.06	1.09	
<b>MAE</b>	1.27	0.83	0.83	0.81	0.82	0.82	0.83	0.82	0.84	0.88	0.84	0.83	0.84	
<b>MB</b>	-1.17	0	-0.03	0	-0.03	0	-0.03	0	-0.03	0.04	-0.02	0	-0.03	
<b>Pearson r<sup>2</sup></b>	0.11	0.1	0.1	0.1	0.1	0.1	0.1	0.1	0.09	0.08	0.1	0.11	0.1	
<b>Spearman r</b>	0.37	0.35	0.37	0.35	0.36	0.34	0.35	0.34	0.34	0.31	0.36	0.36	0.35	
<b>MAX</b>														
<b>RMSE</b>	1.65	1.63	1.82	1.6	1.81	1.6	1.8	1.6	1.8	1.67	1.82	1.6	1.8	
<b>MAE</b>	1.32	1.25	1.33	1.23	1.31	1.23	1.31	1.23	1.31	1.29	1.34	1.23	1.31	
<b>MB</b>	-0.41	0	0.49	0	0.5	0	0.5	0.01	0.49	-0.01	0.49	0.01	0.5	
<b>Pearson r<sup>2</sup></b>	0.09	0.07	0.04	0.08	0.05	0.09	0.05	0.09	0.05	0.06	0.04	0.09	0.05	
<b>Spearman r</b>	0.32	0.27	0.23	0.29	0.24	0.31	0.25	0.3	0.26	0.25	0.22	0.31	0.26	

Average model's bias correction of daily min temperature after 25 bootstrap



528 FIG. B2. Average modelled daily minimum air temperature at 2 m against observed at citizens' personal weather  
 529 stations locations show that all machine learning regressors perform a similar bias-correction on average. In blue,  
 530 modelled temperatures at 2 m are from the model simulation that used the Yonsei University (YSU) planetary  
 531 boundary layer scheme before the bias correction (circles), after the summer time-mean bias correction (squares)  
 532 and after the daily time-step bias correction (stars). In purple, the same values are given for the simulation which  
 533 used the Bougeault-Lacarrère (BouLac) scheme. Dashed lines represent the least squares polynomial fitted lines  
 534 and the black full line represents the identity line.

Average model's bias correction of daily max temperature after 25 bootstrap

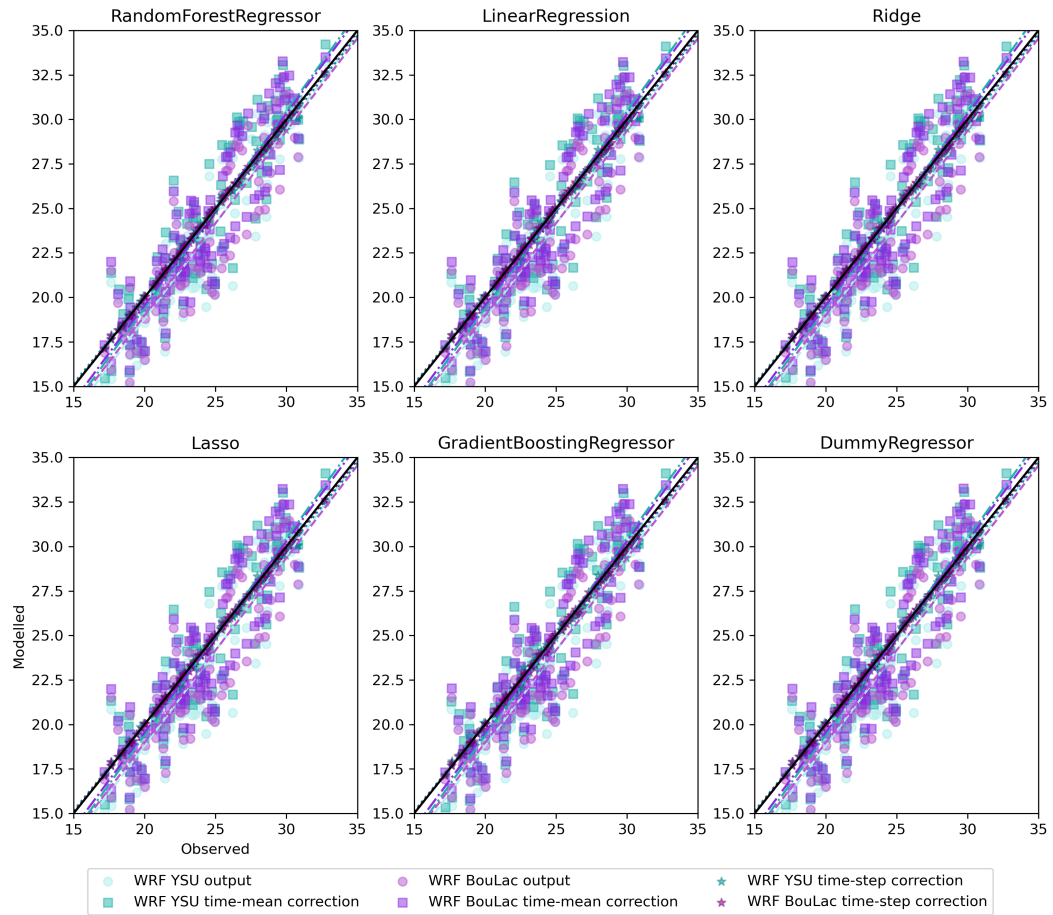


FIG. B3. Same as figure B2, but for daily maximum temperatures.

Average model's bias correction of daily mean temperature after 25 bootstrap

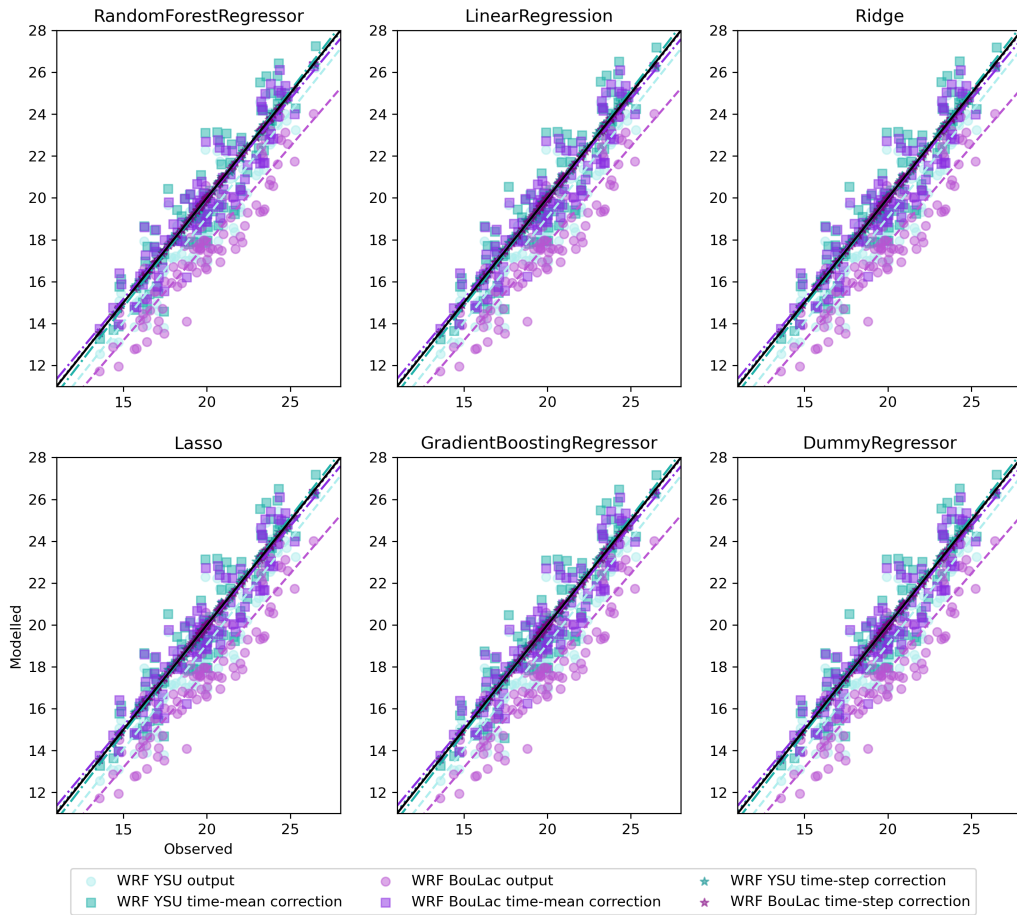


FIG. B4. Same as figure B2, but for daily mean temperatures.

Modelled temperatures and respective bias-corrections with multiple regressors

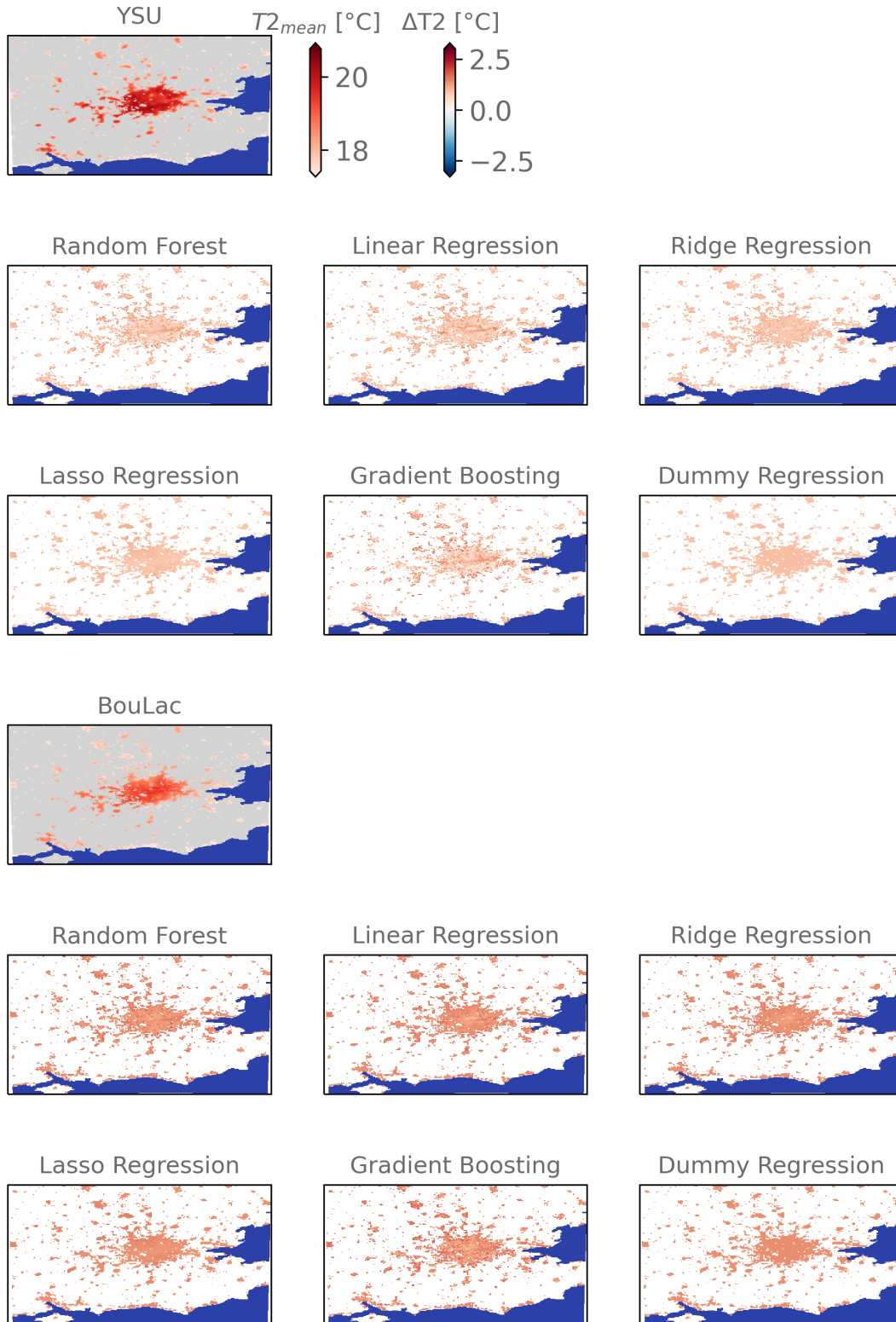


FIG. B5. Same as figure 5, but for daily mean temperatures.

Modelled temperatures and respective bias-corrections with multiple regressors

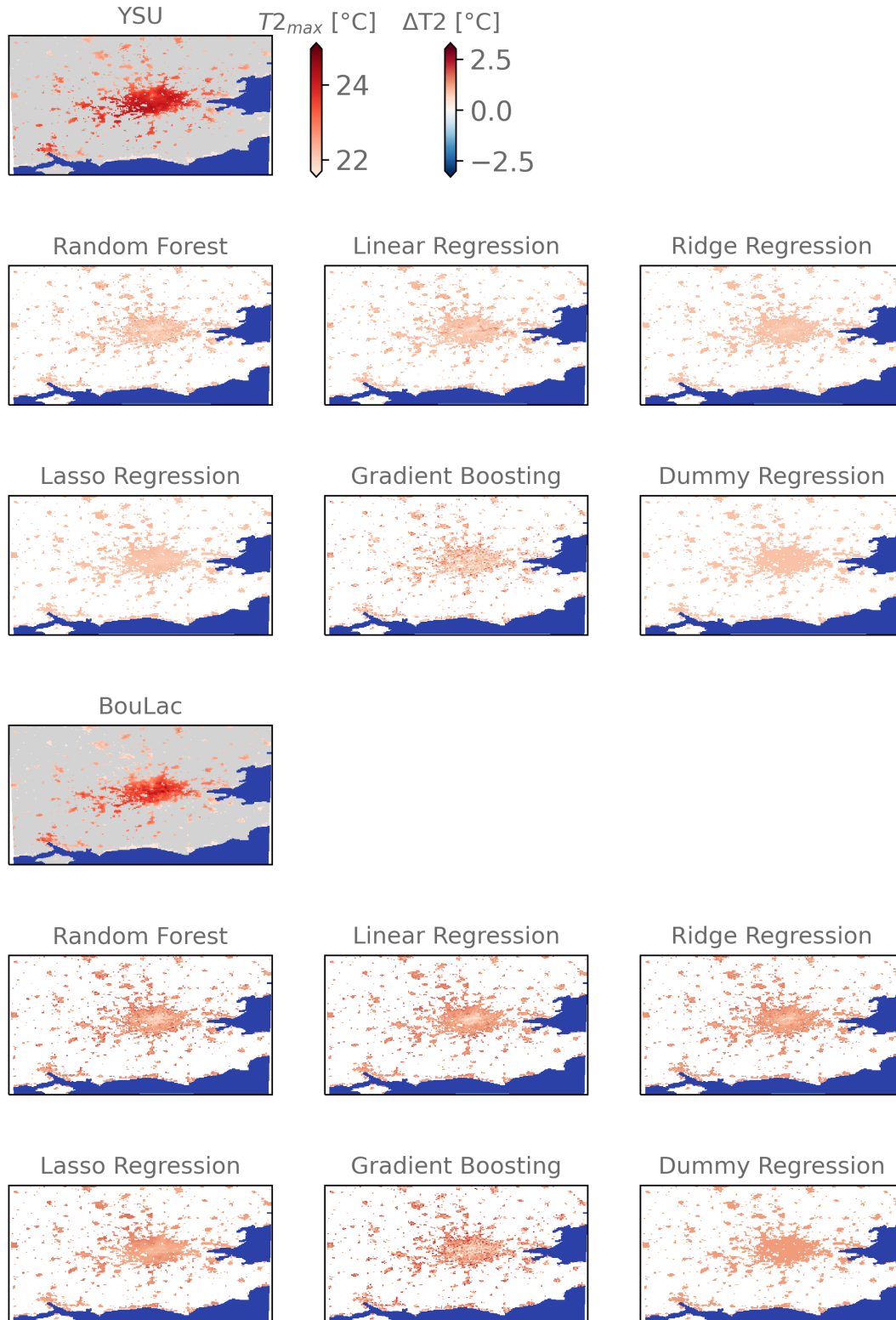


FIG. B6. Same as figure 5, but for daily maximum temperatures.

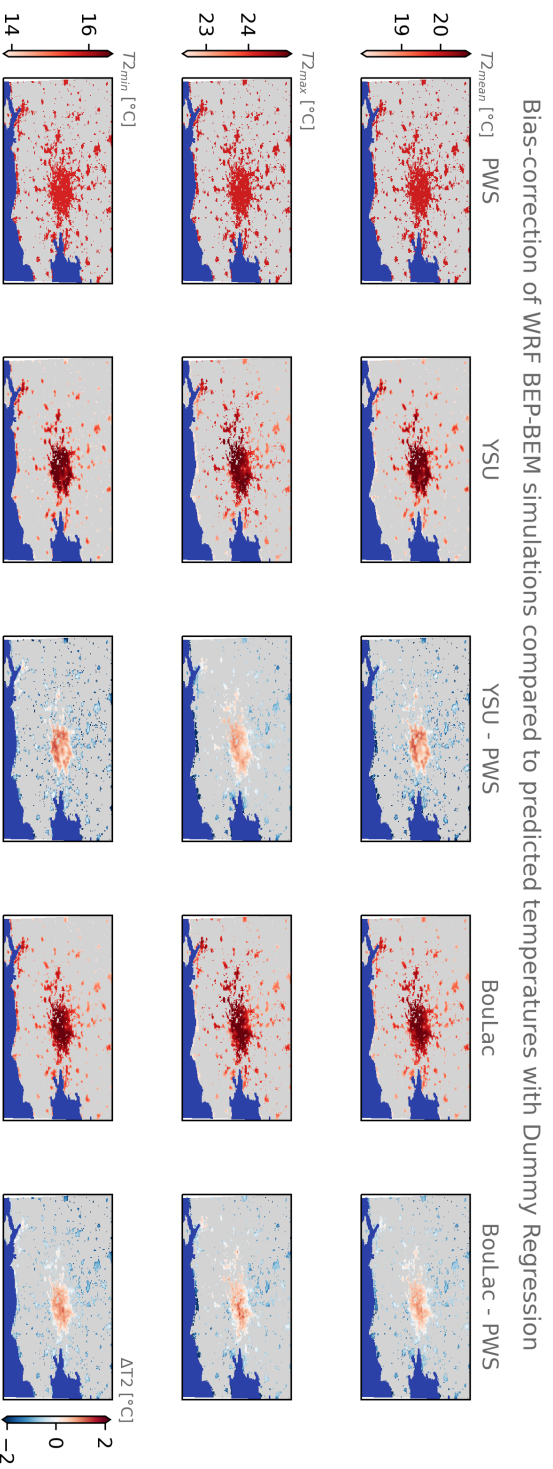


Fig. B7. Same as figure 6, but for dummy regression.

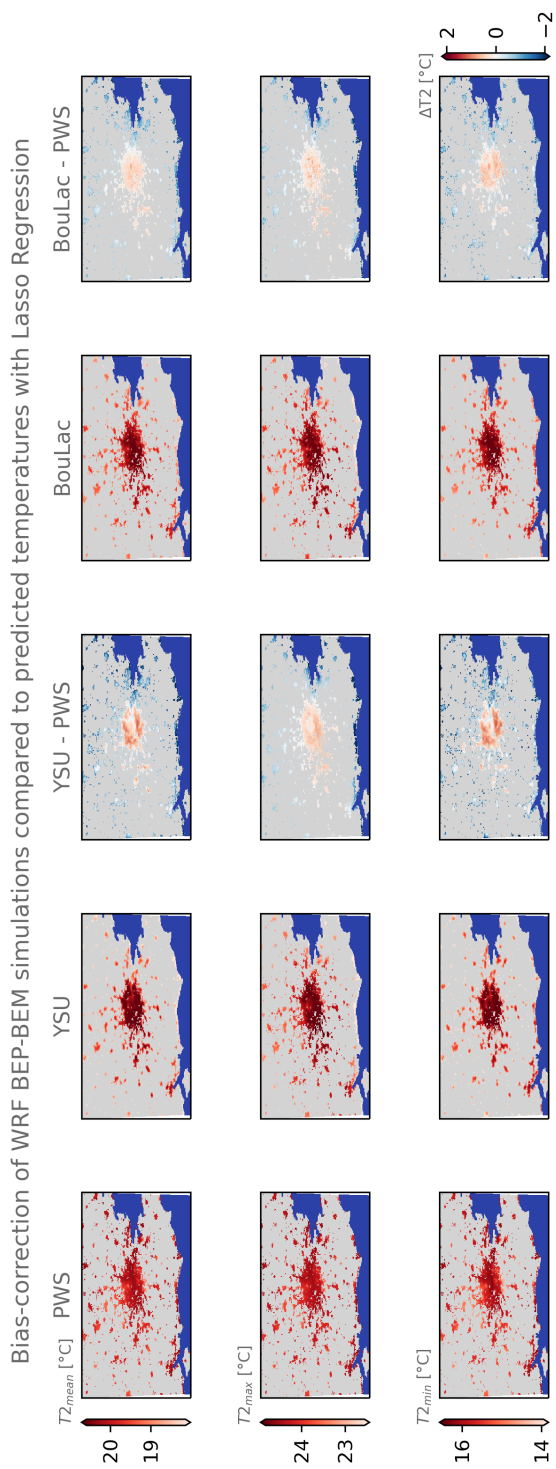


FIG. B8. Same as figure 6, but for Lasso regression.

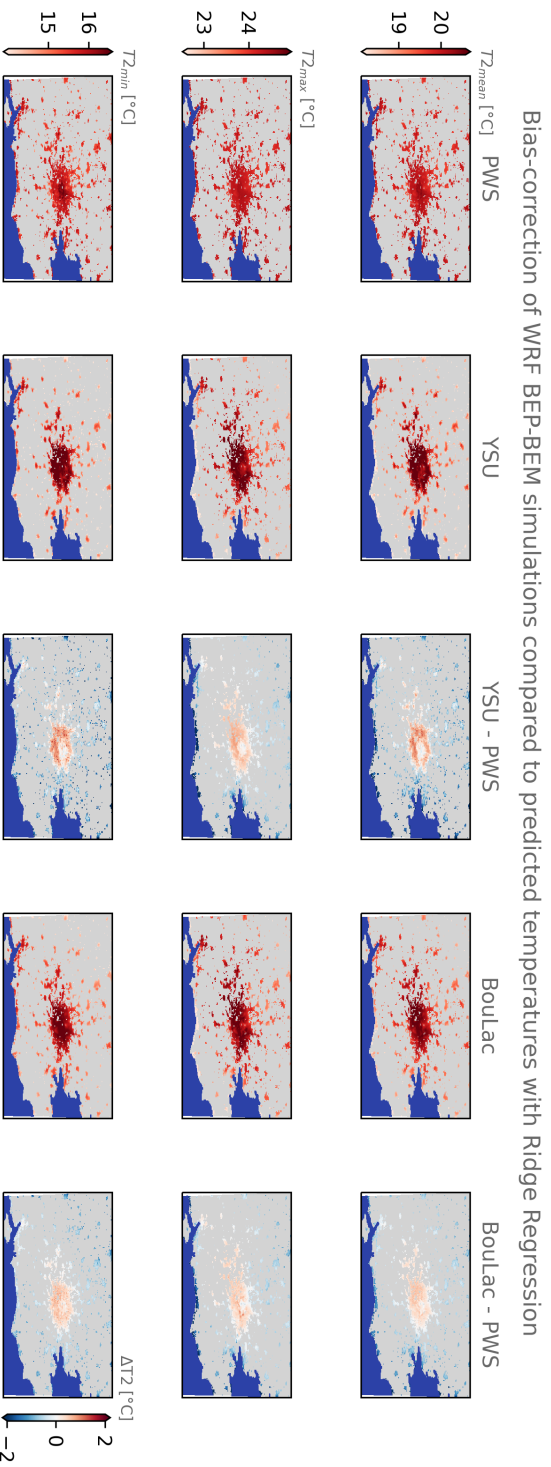


FIG. B9. Same as figure 6, but for Ridge regression.

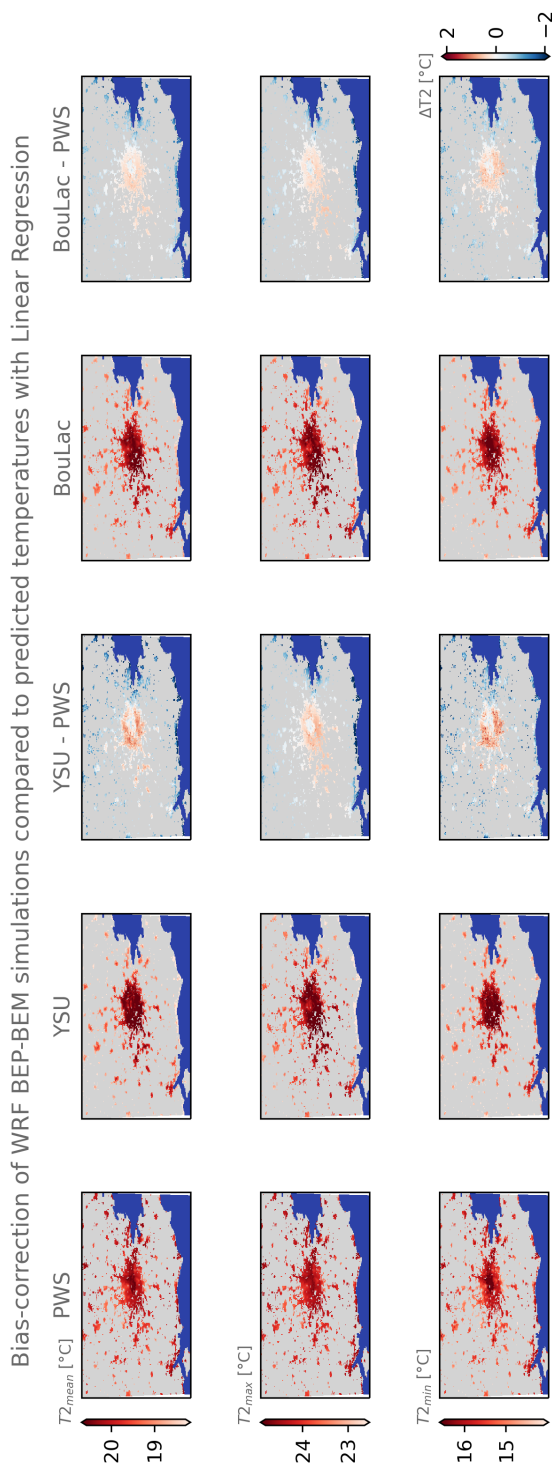


FIG. B10. Same as figure 6, but for linear regression.

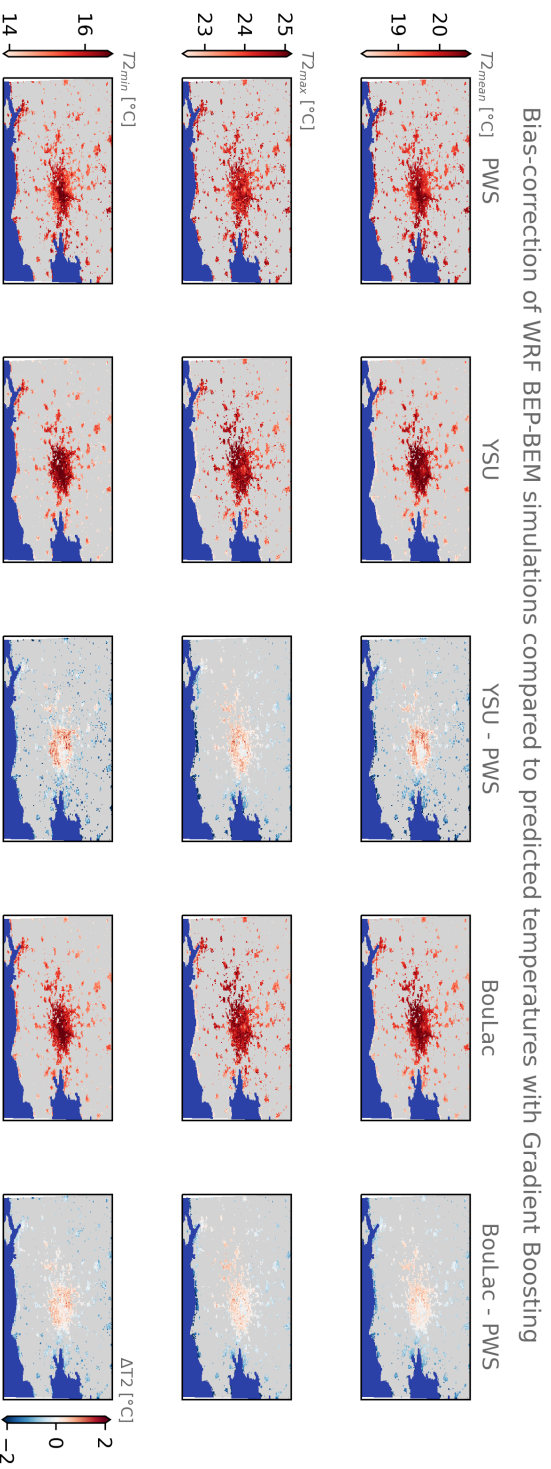


FIG. B11. Same as figure 6, but for gradient boosting regression.

## 535 **References**

- 536 Bassett, R., P. Young, G. Blair, F. Samreen, and W. Simm, 2020: A large ensemble approach to  
537 quantifying internal model variability within the wrf numerical model. *Journal of Geophysical*  
538 *Research: Atmospheres*, **125** (7), e2019JD031 286.
- 539 Benjamin, K., Z. Luo, and X. Wang, 2021: Crowdsourcing urban air temperature data for estimating  
540 urban heat island and building heating/cooling load in london. *Energies*, **14** (16), 5208.
- 541 Bougeault, P., and P. Lacarrere, 1989: Parameterization of orography-induced turbulence in a  
542 mesobeta–scale model. *Monthly weather review*, **117** (8), 1872–1890.
- 543 Brisson, E., M. Demuzere, and N. Van Lipzig, 2015: Modelling strategies for performing  
544 convection-permitting climate simulations. *Meteorologische Zeitschrift*, **25** (2), 149–163.
- 545 Broadbent, A. M., J. Declet-Barreto, E. S. Krayenhoff, S. L. Harlan, and M. Georgescu, 2022:  
546 Targeted implementation of cool roofs for equitable urban adaptation to extreme heat. *Science*  
547 *of the Total Environment*, **811**, 151 326.
- 548 Brousse, O., A. Martilli, M. Foley, G. Mills, and B. Bechtel, 2016: Wudapt, an efficient land use  
549 producing data tool for mesoscale models? integration of urban lcz in wrf over madrid. *Urban*  
550 *Climate*, **17**, 116–134.
- 551 Brousse, O., C. Simpson, N. Walker, D. Fenner, F. Meier, J. Taylor, and C. Heaviside, 2022:  
552 Evidence of horizontal urban heat advection in london using six years of data from a citizen  
553 weather station network. *Environmental Research Letters*, **17** (4), 044 041.
- 554 Chapman, L., C. Bell, and S. Bell, 2017: Can the crowdsourcing data paradigm take atmospheric  
555 science to a new level? a case study of the urban heat island of london quantified using netatmo  
556 weather stations. *International Journal of Climatology*, **37** (9), 3597–3605.
- 557 Ching, J., and Coauthors, 2018: Wudapt: An urban weather, climate, and environmental modeling  
558 infrastructure for the anthropocene. *Bulletin of the American Meteorological Society*, **99** (9),  
559 1907–1924.

560 Demuzere, M., D. Argüeso, A. Zonato, and J. Kittner, 2021: W2w: A python package that  
561 injects wudapt’s local climate zone information in wrf (version v0.1.1). Retrieved online, <https://pypi.org/project/w2w/>.  
562

563 Demuzere, M., B. Bechtel, A. Middel, and G. Mills, 2019: Mapping europe into local climate  
564 zones. *PloS one*, **14** (4), e0214474.

565 Demuzere, M., J. Kittner, A. Martilli, G. Mills, C. Moede, I. D. Stewart, J. van Vliet, and B. Bechtel,  
566 2022: A global map of local climate zones to support earth system modelling and urban scale  
567 environmental science. *Earth System Science Data Discussions*, 1–57.

568 Demuzere, M., and Coauthors, 2017: Impact of urban canopy models and external parameters on  
569 the modelled urban energy balance in a tropical city. *Quarterly Journal of the Royal Meteorological Society*, **143** (704), 1581–1596.  
570

571 Dudhia, J., 1989: Numerical study of convection observed during the winter monsoon experiment  
572 using a mesoscale two-dimensional model. *Journal of Atmospheric Sciences*, **46** (20), 3077–  
573 3107.

574 Fenner, D., B. Bechtel, M. Demuzere, J. Kittner, and F. Meier, 2021: Crowdqc+—a quality-control  
575 for crowdsourced air-temperature observations enabling world-wide urban climate applications.  
576 *Frontiers in Environmental Science*, 553.

577 Fenner, D., A. Holtmann, F. Meier, I. Langer, and D. Scherer, 2019: Contrasting changes of urban  
578 heat island intensity during hot weather episodes. *Environmental Research Letters*, **14** (12),  
579 124013.

580 Fenner, D., F. Meier, B. Bechtel, M. Otto, and D. Scherer, 2017: Intra and inter ‘local climate  
581 zone’ variability of air temperature as observed by crowdsourced citizen weather stations in  
582 berlin, germany. *10.14279/depositonce-10378*.

583 Georganos, S., and Coauthors, 2021: Geographical random forests: a spatial extension of the  
584 random forest algorithm to address spatial heterogeneity in remote sensing and population  
585 modelling. *Geocarto International*, **36** (2), 121–136.

586 Grassmann, T., A. Napoly, F. Meier, and D. Fenner, 2018: Quality control for crowdsourced data  
587 from cws.

- 588 Grimmond, C. S. B., and Coauthors, 2011: Initial results from phase 2 of the international urban  
589 energy balance model comparison. *International Journal of Climatology*, **31** (2), 244–272.
- 590 Gutiérrez, E., J. E. González, A. Martilli, R. Bornstein, and M. Arend, 2015: Simulations of a  
591 heat-wave event in new york city using a multilayer urban parameterization. *Journal of Applied  
592 Meteorology and Climatology*, **54** (2), 283–301.
- 593 Hammerberg, K., O. Brousse, A. Martilli, and A. Mahdavi, 2018: Implications of employing  
594 detailed urban canopy parameters for mesoscale climate modelling: a comparison between  
595 wudapt and gis databases over vienna, austria. *International Journal of Climatology*, **38**, e1241–  
596 e1257.
- 597 Heaviside, C., X.-M. Cai, and S. Vardoulakis, 2015: The effects of horizontal advection on the  
598 urban heat island in birmingham and the west midlands, united kingdom during a heatwave.  
599 *Quarterly Journal of the Royal Meteorological Society*, **141** (689), 1429–1441.
- 600 Hendricks, E. A., J. C. Knierel, and Y. Wang, 2020: Addition of multilayer urban canopy models to  
601 a nonlocal planetary boundary layer parameterization and evaluation using ideal and real cases.  
602 *Journal of Applied Meteorology and Climatology*, **59** (8), 1369–1392.
- 603 Hollis, D., M. McCarthy, M. Kendon, T. Legg, and I. Simpson, 2019: Haduk-grid—a new uk  
604 dataset of gridded climate observations. *Geoscience Data Journal*, **6** (2), 151–159.
- 605 Hong, S.-Y., J. Dudhia, and S.-H. Chen, 2004: A revised approach to ice microphysical processes  
606 for the bulk parameterization of clouds and precipitation. *Monthly weather review*, **132** (1),  
607 103–120.
- 608 Hong, S.-Y., and S.-W. Kim, 2008: Stable boundary layer mixing in a vertical diffusion scheme.  
609 *18th Symposium on Boundary Layers and Turbulence B*, Vol. 16, 325.
- 610 Hong, S.-Y., Y. Noh, and J. Dudhia, 2006: A new vertical diffusion package with an explicit  
611 treatment of entrainment processes. *Monthly weather review*, **134** (9), 2318–2341.
- 612 Janić, Z. I., 2001: Nonsingular implementation of the mellor-yamada level 2.5 scheme in the ncep  
613 meso model.

- 614 Janjić, Z. I., 1994: The step-mountain eta coordinate model: Further developments of the con-  
615 vection, viscous sublayer, and turbulence closure schemes. *Monthly weather review*, **122** (5),  
616 927–945.
- 617 Jiménez, P. A., J. Dudhia, J. F. González-Rouco, J. Navarro, J. P. Montávez, and E. García-  
618 Bustamante, 2012: A revised scheme for the wrf surface layer formulation. *Monthly weather*  
619 *review*, **140** (3), 898–918.
- 620 Kain, J. S., 2004: The kain–fritsch convective parameterization: an update. *Journal of applied*  
621 *meteorology*, **43** (1), 170–181.
- 622 Lauwaet, D., H. Hooyberghs, B. Maiheu, W. Lefebvre, G. Driesen, S. Van Looy, and K. De Ridder,  
623 2015: Detailed urban heat island projections for cities worldwide: dynamical downscaling  
624 cmip5 global climate models. *Climate*, **3** (2), 391–415.
- 625 Lipson, M., S. Grimmond, and M. Best, 2021: Urban-plumber model evaluation project: initial  
626 results. *EGU General Assembly Conference Abstracts*, EGU21–15 230.
- 627 Loridan, T., and C. Grimmond, 2012: Multi-site evaluation of an urban land-surface model: Intra-  
628 urban heterogeneity, seasonality and parameter complexity requirements. *Quarterly Journal of*  
629 *the Royal Meteorological Society*, **138** (665), 1094–1113.
- 630 Maraun, D., and M. Widmann, 2018: *Statistical downscaling and bias correction for climate*  
631 *research*. Cambridge University Press.
- 632 Martilli, A., A. Clappier, and M. W. Rotach, 2002: An urban surface exchange parameterisation  
633 for mesoscale models. *Boundary-layer meteorology*, **104** (2), 261–304.
- 634 Martilli, A., and Coauthors, 2021: Simulating the meteorology during persistent wintertime  
635 thermal inversions over urban areas. the case of madrid. *Atmospheric Research*, **263**, 105 789.
- 636 Masson, V., 2000: A physically-based scheme for the urban energy budget in atmospheric models.  
637 *Boundary-layer meteorology*, **94** (3), 357–397.
- 638 McCarthy, M., and Coauthors, 2019: Drivers of the uk summer heatwave of 2018. *Weather*, **74** (11),  
639 390–396.

640 Meier, F., D. Fenner, T. Grassmann, M. Otto, and D. Scherer, 2017: Crowdsourcing air temperature  
641 from citizen weather stations for urban climate research. *Urban Climate*, **19**, 170–191.

642 Mlawer, E. J., S. J. Taubman, P. D. Brown, M. J. Iacono, and S. A. Clough, 1997: Radiative transfer  
643 for inhomogeneous atmospheres: Rrtm, a validated correlated-k model for the longwave. *Journal*  
644 *of Geophysical Research: Atmospheres*, **102 (D14)**, 16 663–16 682.

645 Mughal, M. O., X.-X. Li, T. Yin, A. Martilli, O. Brousse, M. A. Dissegna, and L. K. Norford,  
646 2019: High-resolution, multilayer modeling of singapore’s urban climate incorporating local  
647 climate zones. *Journal of Geophysical Research: Atmospheres*, **124 (14)**, 7764–7785.

648 Muller, C., L. Chapman, S. Johnston, C. Kidd, S. Illingworth, G. Foody, A. Overeem, and R. Leigh,  
649 2015: Crowdsourcing for climate and atmospheric sciences: current status and future potential.  
650 *International Journal of Climatology*, **35 (11)**, 3185–3203.

651 Napoly, A., T. Grassmann, F. Meier, and D. Fenner, 2018: Development and application of a  
652 statistically-based quality control for crowdsourced air temperature data. *Frontiers in Earth*  
653 *Science*, **6**, 118.

654 Nazarian, N., and Coauthors, 2022: Integrated assessment of urban overheating impacts on human  
655 life. *Earth’s Future*.

656 Niu, G.-Y., and Coauthors, 2011: The community noah land surface model with multiparameteri-  
657 zation options (noah-mp): 1. model description and evaluation with local-scale measurements.  
658 *Journal of Geophysical Research: Atmospheres*, **116 (D12)**.

659 Oke, T. R., G. Mills, A. Christen, and J. A. Voogt, 2017: *Urban climates*. Cambridge University  
660 Press.

661 Oleson, K., G. Anderson, B. Jones, S. McGinnis, and B. Sanderson, 2018: Avoided climate impacts  
662 of urban and rural heat and cold waves over the us using large climate model ensembles for rcp8.  
663 5 and rcp4. 5. *Climatic change*, **146 (3)**, 377–392.

664 Pedregosa, F., and Coauthors, 2011: Scikit-learn: Machine learning in python. *the Journal of*  
665 *machine Learning research*, **12**, 2825–2830.

- 666 Potgieter, J., N. Nazarian, M. J. Lipson, M. A. Hart, G. Ulpiani, W. Morrison, and K. Benjamin,  
667 2021: Combining high-resolution land use data with crowdsourced air temperature to investigate  
668 intra-urban microclimate. *Frontiers in Environmental Science*, 385.
- 669 Salamanca, F., A. Krpo, A. Martilli, and A. Clappier, 2010: A new building energy model coupled  
670 with an urban canopy parameterization for urban climate simulations—part i. formulation,  
671 verification, and sensitivity analysis of the model. *Theoretical and applied climatology*, **99 (3)**,  
672 331–344.
- 673 Salamanca, F., and A. Martilli, 2010: A new building energy model coupled with an urban canopy  
674 parameterization for urban climate simulations—part ii. validation with one dimension off-line  
675 simulations. *Theoretical and Applied Climatology*, **99 (3)**, 345–356.
- 676 Salamanca, F., A. Martilli, M. Tewari, and F. Chen, 2011: A study of the urban boundary layer  
677 using different urban parameterizations and high-resolution urban canopy parameters with wrf.  
678 *Journal of Applied Meteorology and Climatology*, **50 (5)**, 1107–1128.
- 679 Salamanca, F., A. Martilli, and C. Yagüe, 2012: A numerical study of the urban heat island over  
680 madrid during the desirex (2008) campaign with wrf and an evaluation of simple mitigation  
681 strategies. *International Journal of Climatology*, **32 (15)**, 2372–2386.
- 682 Sgoff, C., W. Acevedo, Z. Paschalidi, S. Ulbrich, E. Bauernschubert, T. Kratzsch, and R. Potthast,  
683 2022: Assimilation of crowd-sourced surface observations over germany in a regional weather  
684 prediction system. *Quarterly Journal of the Royal Meteorological Society*.
- 685 Stewart, I. D., and T. R. Oke, 2012: Local climate zones for urban temperature studies. *Bulletin of*  
686 *the American Meteorological Society*, **93 (12)**, 1879–1900.
- 687 Stewart, I. D., T. R. Oke, and E. S. Krayenhoff, 2014: Evaluation of the ‘local climate zone’ scheme  
688 using temperature observations and model simulations. *International journal of climatology*,  
689 **34 (4)**, 1062–1080.
- 690 Sunter, M., 2021: Midas data user guide for uk land observations, v20210705.
- 691 Tewari, M., F. Salamanca, A. Martilli, L. Treinish, and A. Mahalov, 2017: Impacts of projected  
692 urban expansion and global warming on cooling energy demand over a semiarid region. *Atmo-*  
693 *spheric Science Letters*, **18 (11)**, 419–426.

694 UKMO, 2021: Midas open: Uk hourly weather observation data, v202107. centre for  
695 environmental data analysis, 08 september 2021. Data retrieved online, doi:10.5285/  
696 3bd7221d4844435dad2fa030f26ab5fd.

697 Varentsov, M., D. Fenner, F. Meier, T. Samsonov, and M. Demuzere, 2021: Quantifying local  
698 and mesoscale drivers of the urban heat island of moscow with reference and crowdsourced  
699 observations. *Frontiers in Environmental Science*, 543.

700 Venter, Z. S., O. Brousse, I. Esau, and F. Meier, 2020: Hyperlocal mapping of urban air temperature  
701 using remote sensing and crowdsourced weather data. *Remote Sensing of Environment*, **242**,  
702 111 791.

703 Venter, Z. S., T. Chakraborty, and X. Lee, 2021: Crowdsourced air temperatures contrast satellite  
704 measures of the urban heat island and its mechanisms. *Science Advances*, **7 (22)**, eabb9569.

705 Virtanen, P., and Coauthors, 2020: Scipy 1.0: fundamental algorithms for scientific computing in  
706 python. *Nature methods*, **17 (3)**, 261–272.

707 Wang, J., and X.-M. Hu, 2021: Evaluating the performance of wrf urban schemes and pbl schemes  
708 over dallas–fort worth during a dry summer and a wet summer. *Journal of Applied Meteorology  
709 and Climatology*, **60 (6)**, 779–798.

710 Wouters, H., M. Demuzere, U. Blahak, K. Fortuniak, B. Maiheu, J. Camps, D. Tielemans, and  
711 N. P. van Lipzig, 2016: The efficient urban canopy dependency parametrization (sury) v1. 0 for  
712 atmospheric modelling: description and application with the cosmo-clm model for a belgian  
713 summer. *Geoscientific Model Development*, **9 (9)**, 3027–3054.

714 Wouters, H., and Coauthors, 2017: Heat stress increase under climate change twice as large in  
715 cities as in rural areas: A study for a densely populated midlatitude maritime region. *Geophysical  
716 Research Letters*, **44 (17)**, 8997–9007.

717 Yang, J., and E. Bou-Zeid, 2019: Scale dependence of the benefits and efficiency of green and cool  
718 roofs. *Landscape and urban planning*, **185**, 127–140.

719 Yang, Z.-L., and Coauthors, 2011: The community noah land surface model with multiparam-  
720 eterization options (noah-mp): 2. evaluation over global river basins. *Journal of Geophysical  
721 Research: Atmospheres*, **116 (D12)**.

- 722 Zängl, G., D. Reinert, P. Rípodas, and M. Baldauf, 2015: The icon (icosahedral non-hydrostatic)  
723 modelling framework of dwd and mpi-m: Description of the non-hydrostatic dynamical core.  
724 *Quarterly Journal of the Royal Meteorological Society*, **141 (687)**, 563–579.
- 725 Zonato, A., A. Martilli, S. Di Sabatino, D. Zardi, and L. Giovannini, 2020: Evaluating the  
726 performance of a novel wudapt averaging technique to define urban morphology with mesoscale  
727 models. *Urban Climate*, **31**, 100 584.
- 728 Zonato, A., A. Martilli, P. A. Jimenez, J. Dudhia, D. Zardi, and L. Giovannini, 2022: A new  $k-\varepsilon$   
729 turbulence parameterization for mesoscale meteorological models. *Monthly Weather Review*.
- 730 Zumwald, M., B. Knüsel, D. N. Bresch, and R. Knutti, 2021: Mapping urban temperature using  
731 crowd-sensing data and machine learning. *Urban Climate*, **35**, 100 739.